# Lamb wave propagation for evaluating defects in structural adhesive joints

*Nuno Filipe Mota Lucas*

**Master dissertation**

Supervisor:
Prof. António Mendes Lopes

Co-supervisor:
Prof. Lucas Filipe Martins da Silva
Inv. Carlos Moreira da Silva
Eng. António Francisco Galhano Tenreiro

U.PORTO
FEUP FACULDADE DE ENGENHARIA
UNIVERSIDADE DO PORTO

**Master in Mechanical Engineering**

**Specialization of Automation**

September, 2020

# Resumo

Atualmente, os adesivos estruturais são cada vez mais usados como alternativa aos métodos clássicos de ligação mecânica, uma vez que contribuem para o aumento da razão entre a resistência e o peso da estrutura, diminuindo o custo, como consequência.

Para uma utilização confiável das juntas adesivas, é necessário garantir que o processo de adesão ocorra de forma adequada. A verificação pode ser feita de duas maneiras: com testes destrutivos ou com testes não destrutivos. Os métodos não destrutivos são mais vantajosos, pois não é necessário danificar nenhuma amostra. Nesta dissertação, é usado o método de ensaios ultrassónico com recurso a *Lamb waves*. Para a análise, recorre-se ao uso de sensores piezoelétricos para poder gerar e captar os sinais de interesse. Este processo é útil em monotorização de integridade estrutural ao longo do tempo de vida da junta, uma vez que os sensores ficam permanentemente instalados, providenciando uma análise contínua.

As amostras analisadas nesta dissertação consistem em juntas de sobreposição simples, de pequenas dimensões, com apenas 25 x 25 $mm^2$ de sobreposição. O objetivo da análise cinge-se na deteção de defeitos na zona colada. O defeito em causa é um vazio localizado dentro da camada de adesivo. Este defeito é bastante comum e deve-se a uma incorreta aplicação do adesivo durante o processo de manufatura da junta. Neste trabalho, o vazio foi criado colando pequenos círculos de fibra de teflon nos substratos, antes da aplicação do adesivo. De modo a poder analisar a existência de defeitos nas juntas de sobreposição simples, foi realizado um conjunto de testes experimentais, onde se compararam juntas com e sem defeito. Finalmente, foram realizados testes destrutivos às amostras, de modo a comprovar a presença do dano.

O estudo experimental foi acompanhado de um estudo numérico em ABAQUS envolvendo, por exemplo, a resposta a diferentes tipos de frequência de excitação, dimensão do dano e a sua localização. Deste modo, dois modelos de provete foram criados. O primeiro foi uma placa de alumínio que, devido a sua simplicidade, foi usado para avaliar como as *Lamb wave*s se propagam com diferentes sinais de atuação. O segundo modelo foi de uma junta de sobreposição simples semelhante às criadas para o procedimento experimental, a fim de comparar os resultados.

Em suma, este método provou ser capaz de detetar os defeitos gerados tanto numericamente como experimentalmente, mais especificamente a presença de vazios embutidos no adesivo, independentemente de seu tamanho ou localização.

# Abstract

Structural adhesives are currently being used as an alternative to classic mechanical bonding methods. They increase the ratio between strength and weight of the structure, reducing its cost as a consequence.

For reliable use of adhesives, it is necessary to ensure that the adhesion process occurs without problems. In this way, different test methods are used: destructive testing or non-destructive testing. Non-destructive tests are more beneficial since it is unnecessary to damage the sample. In this dissertation, the ultrasonic test method utilizing Lamb waves was used to analyse the samples. Piezoelectric sensors were used to generate and capture the Lamb waves. This process is useful in structural health monitoring since the sensors are permanently attached to the structure and enable a continuous analysis.

The samples analysed in this dissertation consist of small single lap joints with 25 x 25 $mm^2$ of overlap. The study's purpose is to understand the effectiveness of Lamb waves to detect defects in the adhesive area. The defect consists of a void located within the adhesive layer. The generation of voids is quite common in real-world adhesive joint manufacturing due to the adhesive's wrongful application during the manufacturing process. In this dissertation, the voids were artificially created by gluing small Teflon fibre circles on the substrates before applying the adhesive. In order to analyse the existence of defects, a set of experimental tests was carried out, in which joints with and without defects were compared. Finally, destructive tests were performed on the samples in order to confirm the presence of damage.

The experimental analysis was accompanied with a numerical study based on ABAQUS, in order to get a broader understanding of the physical phenomenon and see the influence of several variables, such as, for example, the sample's response to the variation of the excitation frequency, the size of the damage, and to the variation of the damage location. As such, two models were created. The first one was a simple aluminium plate model, used to evaluate how Lamb waves respond to different actuation signals. The second model corresponds to a single lap joint, similar to the specimens created for the experimental procedure, to compare the results.

In short, this method has proven to be able to detect defects, more specifically the presence of voids embedded in the adhesive, despite their size or location.

# Acknowledgments

First, I would like to manifest my gratitude to my supervisor, Prof. António Mendes Lopes, for the opportunity to be a part of this project and for the knowledge and expertise shared throughout this project.

A special thanks to my co-supervisors, Prof. Lucas da Silva, Prof. Carlos Moreira da Silva, and Eng. Francisco Tenreiro, for the guidance, the knowledge shared, the long hours of work, and constant availability and patience to help me along with this project.

I would also like to express my gratitude to the Advance Joining Processes Unit, AJPU, at INEGI, and all his members for the constant availability. All the knowledge and time bestowed helping me during this project; without their guidance, this project would not have been possible.

To my family, who always supported me and raised me to be the best version of myself, and who taught me never to give up, even in the darkest times.

To my girlfriend, Joana Tribuzi, who stood by my side through all these days for the past five years, always finding ways to help me.

To my friends, the ones who always believed in me and spent countless hours studying with me, I am eternally grateful for all of you.

# Contents

# List of Figures

# List of Tables

# List of acronyms

LW- Lamb waves

SLJ- Single lap joint

NDT- Non-destructive test

SHM- Structural health monitoring

PZT- Piezoelectric

VT- Visual and optical testing

LPI- Penetrant liquid inspection

MPI-Magnetic particle testing

ET- Electromagnetic testing

UT- Ultrasonic testing

RT- Radiography

UV- Ultraviolet

$C_g$ - Group velocity

$C_l$ – Phase velocity

# 1 Introduction

## 1.1 Background and motivation

Adhesives are increasingly being used in various industries such as automotive, aeronautical, and aerospace, because of their unique advantages compared to conventional mechanical joining methods. Bonded Joints have been replacing standard joining methods in various vehicular products, lowering their weight, and, consequently, allowing for lower energy consumption and fewer emissions. Furthermore, they allow a more uniform stress distribution, which leads to good resistance to fatigue, higher stiffness, better load transmission, the ability to bond dissimilar materials, and different geometries. The easiness of the automatic process provides a faster and more cost-efficient process and design flexibility. The adhesives are used to create structural adhesive joints capable of bearing high loads as requested by the automotive, aeronautical, and aerospace industries.

There are two distinct ways of determining a specimen's integrity: by a destructive test or a non-destructive test (NDT). In destructive testing, tests are carried out to the specimen's failure to understand a specimen's performance or material behaviour under different loads. These tests are generally much easier to implement, yield more information, and are easier to interpret than NDT. Interpreting and documenting the destructive failure mode is frequently achieved using a high-speed camera recording until the failure is detected. Detecting the failure can be achieved using a sound detector or stress gauge, which produces a signal to trigger the high-speed camera.

On the other hand, to monitor structural adhesive joints' integrity, the industry resorts to NDT. NDT can be a useful tool for evaluating bonded joint's quality, since it does not require its destruction and saves money and time in product evaluation, troubleshooting, and research. In NDT methods, structural reliability is examined periodically by external sources such as ultrasound or X-ray. On the other hand, a unique characterization approach and damage detection techniques are performed in structural health monitoring (SHM) to evaluate mechanical structure anomaly. In SHM, there is no need for any external operator because

sensors and actuators are attached to the examined structure permanently to continuously obtain the monitored data during all the structure's working hours. SHM verifies the present condition and the expected efficiency, which helps make decisions about the required maintenance and safety of structural systems. Design parameters and safety of a mechanical structure can be improved through SHM. Real SHM involves NDT, sensor technology, data acquisition, damage initiation mechanics, and signal processing. Sensing devices with accuracy and high sensitivity play a vital role in SHM systems, like the piezoelectric sensors. To avoid any tragic failure, this continuous monitoring of a system will enhance the probability of damage detection.

There are many NDT methods, each with their unique set of techniques to detect defects. However, this dissertation will be focusing on ultrasonic testing (UT) since it is the baseline of the work developed by the SHM carried out. The UT uses pulse waves with frequencies up to 50 MHz to detect internal defects. The use of Lamb waves (LW) in UT is a new and promising tool for damage detection. The possibility of an improper application of the adhesive during the manufacturing process results in defects, thus changing the idealized joint properties. Therefore, with the use of piezoelectric elements as actuator and sensor, one can excite and detect LW, as well as their change in behaviour due to the presence of damage.

The data obtained by the piezoelectric (PZT) sensors can be analysed and interpreted, resorting to various techniques. The data can be analysed in two different domains, time or frequency and depending on which domain the data is being analysed, the method used also varies. In the time domain, it is typically used damage indices and the RAPID (Reconstruction Algorithm for the Probabilistic Inspection of Damage). In the frequency domain, one can resort to methods like the Fourier transform.

## 1.2 Objectives

This dissertation has two main objectives. The first is to analyse de data recorded by the piezoelectric sensors to detect the defect embedded in the adessive layer by resorting to LW. This analysis will be done by comparing the results in a time domain of both specimens with and without defect.

The second objective consists of creating a numerical model to expand the number of tests and better understand how LW propagates through a single lap joint (SLJ).

## 1.3 Research methodology

The objectives for the conclusion of this dissertation were accomplished by performing the following steps:

- A thorough literature review focused on this dissertation three main topics: adhesives, non-destructive testing methods, and LW.
- A numerical model of an aluminium plate with 2 mm thickness was created in ABAQUS in order to test how LW works and how different variables, such as frequency, mesh size, or step time, impact the simulation.
- The numerical model of a SLJ was developed to enlarge the number of tests that could be performed experimentally and test the best scenarios to perform experimentally.
- Experimental tests were carried out with different void sizes to achieve reliable proof that the NDT method detects structural adhesive joints' defects. An experimental test with bad adhesion (also known as kissing bond) was also performed.
- Destructive tests were carried onto the specimens to verify if the defects were created as expected and confirm the conclusions taken regarding the experimental work results.

## 1.4 Dissertation outline

This dissertation is divided into five main parts.

Chapter 1 contains a brief introduction to the main problem as well as the objectives and the research methodology used.

Chapter 2 consists of a literature review of three topics: adhesive joints, NDT technologies for bonded joints, and LW. Regarding adhesives joints, their classification, their advantages and disadvantages, and their most common failure modes and designs are considered. Afterward, a historical perspective of NDT methods is presented. Finally, LW are addressed since to analyse the data, it is essential to understand how these waves propagate, their nature, and how one can interpret the measured waves to detect damage.

Chapter 3 presents all the experimental work and equipment used during this dissertation and the results of all experiments made to determine the presence of a defect in a bonded joint.

Chapter 4 explains the finite element model created to analyse LW's behaviour using a single model (aluminium plate) and a model of a SLJ.

Chapter 5 outlines the conclusions regarding the results from chapters 3 and 4 and presents suggestions and further works on these topics.

# 2 Literature review

## 2.1 Adhesives

Synthetic polymers have properties that allow them to adhere to most materials easily and have a strength capable of transmitting considerable loads.

According to Kinloch [1], an adhesive can be defined as a material that can join two other specimens and resist their separation. Other substances, such as inks and printing inks, are outside this definition, but illustrate the phenomenon of adhesion. A structural adhesive can be defined as an adhesive that can withstand substantial loads, being responsible for the structure's strength, and rigidity [2].

Adhesives have been used for centuries. The majority were obtained from natural products, such as bones, skins, fish, and milk, but nowadays, they are based on synthetic polymers, such as epoxy resins, and they can be seen as a type of glue, cement, or paste [3].

The materials to be joined are called substrates. Alternatively, they can be called adherends after the bonding procedure has been performed. Both sealants and adhesives work by adhesion phenomena. Adhesion can be defined as the attraction between two substances resulting from intermolecular forces established between them. This concept is different from that of cohesion, which only involves intermolecular forces within a substance. The main molecular forces that exist in adhesion and cohesion are mostly Van der Waals forces [4].

Materials bonded with sealants or adhesives break through cohesion, adhesion, or a combination of the two. The interphase is the region between the adherends and the adhesive. The nature of the interphase is critical in determining the mechanical properties of the adhesive. The interface is within the interphase and is a contact plane between the surface and the two materials, often called a boundary layer. The joint is then formed by the adherents, the adhesive or sealant, and the interfaces and interphase [4].

Adhesives are materials designed to hold components together with the same, or different, characteristics by surface attraction, often as alternatives to mechanical fastening systems, such as nuts and bolts, rivets, or welding and soldering [5].

There are two main types of adhesive bonding: structural and non-structural. Structural adhesive bonding is used for applications in which the adherends (the objects being bonded) may experience large stresses up to their yield point. Structural adhesive bonds must be capable of transmitting stress without loss of integrity within design limits [6,7].

The use of adhesives comes with a wide variety of advantages when compared with mechanical fasteners, such as:

- They provide a more uniform stress distribution along the bonded area, enabling a higher stiffness and load transmission, reducing weight and cost (Figure 2.1) ;
- Due to the polymeric nature of the adhesive, adhesive joints provide excellent damping properties, which also enable them to have high fatigue strength;
- Adhesives can bond dissimilar materials with different thermal expansion coefficients because the adhesive flexibility can compensate for the difference;
- They bond thin plates very efficiently, which is one of the significant applications of structural adhesives;
- Adhesives have a strength well below that of metals. However, when used on thin bond plates with a large bearing area, the adhesive strength is enough for structural applications;
- The adhesive application can be very efficient because it is easy to create an automatic process;
- The joint design is very flexible, enabling new design concepts and materials to be introduced;
- Adhesives enable them to have very smooth surface finishes because they avoid holes for rivets, bolts, or welding marks;
- They create intimate contact between the bonded surfaces, which is useful in structural terms and corrosion resistance;
- Adhesive assembly is often much faster and more cost-effective than a mechanical method [4,5].

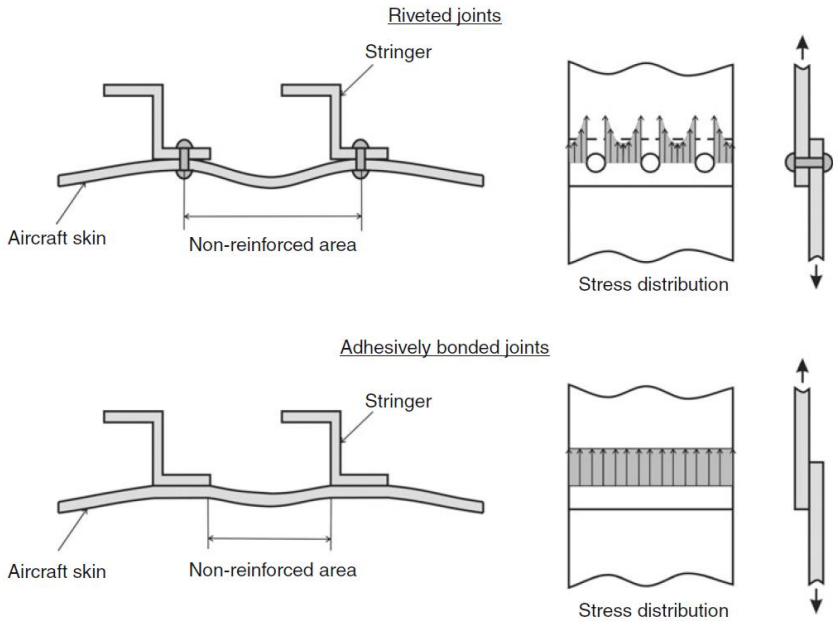


Figure 2.1: Comparison between riveted and adhesively bonded joints in terms of stiffness (left) and stress distribution (right) [4].

However, adhesive joints also have some disadvantages that should be accountable for:

- The existence of peel and cleavage stress create a load concentration in a small area, resulting in low strength;
- High atmospheric humidity and temperature cycles can cause hygrothermal aging in adhesives, which result in the degradation of their mechanical properties;
- They need structures to maintain the substrates in position, such as molds since the bonding is not instantaneous;
- They require meticulous surface preparation to ensure good adhesion;
- The necessity of temperature for the hardening of a wide variety of adhesives;
- The process of quality control in adhesive joints can be cumbersome and flawed. Therefore, unwanted defects that originate in the manufacturing process must be detected [4, 5].

## 2.2 Adhesive Classification

The adhesives can be classified according to their polymer base, functionality in the polymer backbone, functional type, chemical family, physical form, and application method [4].

The polymer base can be synthetic or natural. Naturally based adhesives include animal and vegetable-based adhesives and natural gums. On the other hand, adhesives with a synthetic base include all adhesives that are not natural [4,8].

The polymer backbone functionality can be thermoplastic, elastomeric, thermosetting, and hybrid. Thermosetting adhesives are polymers that cure due to chemical reactions at room or high temperature, which cannot be heated and melted after initial curing. They can be supplied as one-part or multi-part systems. The one-part system usually has a short service life and requires a high temperature to cure. Multi-part systems usually have a longer service life and cure at room temperature. Thermoplastic adhesives are cured from melting or solvent loss and can be melted without significantly altering their properties. Elastomeric polymers typically have a higher elongation, toughness, and peel strength. The hybrid adhesives result from a combination of any of the previous [4,8].

The physical form generally defines how the adhesive should be applied and can be liquid, powder, film, or paste. Liquid adhesives can be applied using rollers, spray, and have good gap-filling capabilities. Paste adhesives can be applied to vertical surfaces as they have high viscosity and a low tendency to drip or sag. The film adhesives ensure that the glue line thickness is constant and easy to handle and use. Powdered adhesives generally need to be heated or dissolved in a solvent to transform them into a liquid form for later application [4,8].

The functional classifier allows for the distinction between structural and non-structural adhesives. The adhesives can also be referred to as hot melt, pressure-sensitive, water-base, ultraviolet/electron beam cured, and conductive [4].

Adhesive can be classified by their chemical composition, such as acrylic, epoxy, polyurethane, among others. Epoxy adhesives are essential in the structural adhesive family and are the most versatile. Thermoset adhesives are strong and fragile. However, they can be formulated to be flexible and resistant without loss of tensile strength. Acrylics provide fast cure and high strength, although they are more expensive than epoxies. Polyurethane is flexible and resistant even at low temperatures, despite its sensitivity to moisture and heat. The application method depends on the viscosity and can be brushing, coating, or spraying [4,8].

### 2.2.1 Failure modes and joint design

Adhesive joints with metallic substrates can have three different failure modes: adhesive (interfacial) failure, cohesive failure in the adhesive, and cohesive failure in the adherend.

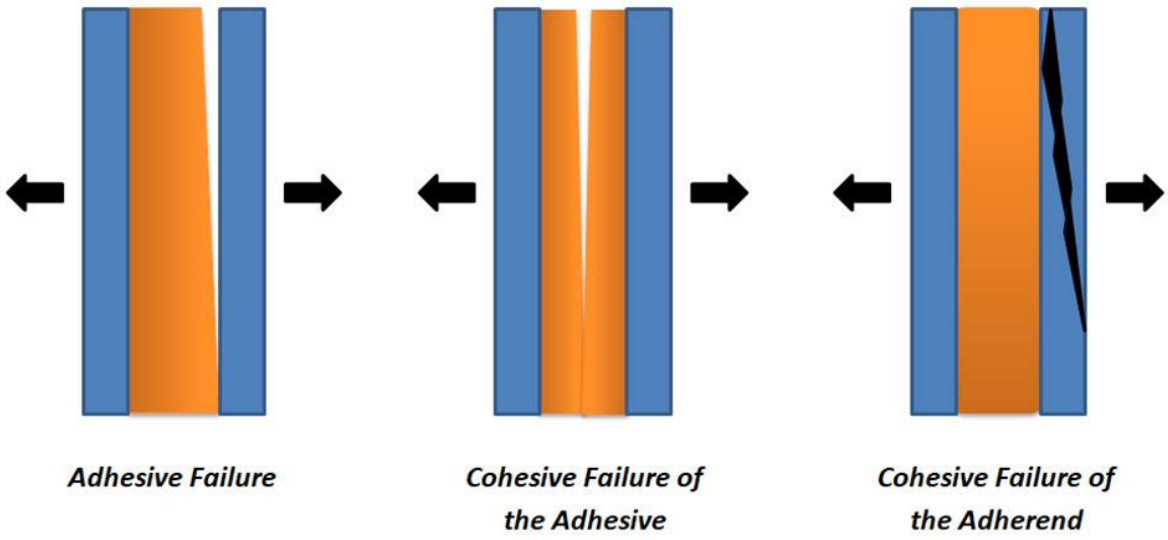


Figure 2.2: Schematic representation of cohesive and adhesive failures[39].

Figure 2.2 shows that when a cohesive failure occurs in the adhesive, both adhesives' surfaces remain covered by the adhesive. This type of failure can happen due to thermal stresses, gross void defects, or inadequate length and overlap. When adhesive failure occurs, the adhesion failure is between one of the adherends and the adhesive, resulting from inadequate surface preparation. Alternatively, when the adhesive bond is comparatively too strong, the adherend reaches its material strength limit and fails before the adhesive bond. This is referred to as cohesive failure in the adherent [4].

### 2.2.2 Adhesive bond failure modes

In an adhesive joint, there are three primary ways in which an adhesive joint can fail:

- in one of the adherends outside the joint
- by fracture of the adhesive layer
- interfacially between the adhesive and one of the adherends (adhesion failure).

Failure of the adherends outside the joint is achievable for well-designed and fabricated adhesive bonds in moderately thin adherend materials. This condition is desirable since it allows the adhesives' excellent structural performance to be used [10].

#### 2.2.2.1 Cohesive failures

Failures in the cohesion bond result in the adhesive fracture and are characterized by adhesive material on the corresponding faces of both adherends. This failure usually occurs by shearing, but peel stresses or a combination of shearing and peeling can also cause cohesion failure. In this type of failure, the adhesive surface usually looks rough and may be lighter in

colour than bulk adhesive material. In adhesive film systems, the failure usually occurs along the plane of the carrier cloth. Cohesion failures encountered in service are usually caused by defective joint design. Excessive or insufficient overlap length can also result in cohesion failure.

Adhesive bonds are very resistant to fatigue, and only under certain circumstances can a cohesive failure be caused by fatigue. As long as the joint has overlap length and a thin adhesive, it is unlikely that connection fatigue will occur.

Fatigue failures in adhesive connections usually occur where the structure being joined is thick, and the loads are high. This phenomenon always occurs in the adhesive and not in the interface, and film adhesives usually propagate through the carrier cloth plane. If a high-power microscope is used, fatigue striations located within the failure surface can be detected, evidenced by fatigue failure [10].

#### 2.2.2.2 Adhesion failure

This type of failure is characterized by the absence of adhesive on one of the bonding surfaces. The adhesion failure occurs due to the hydration of the chemical bonds that form the bond between the surface and the adhesive, and it occurs along with the interface between the adhesive layer and one of the adherends.

There are three causes of adhesion failure:

- Use of an inadequate surface preparation technique that cannot produce a chemically active surface resistant to hydration.
- The adhesive had already cured before the bond was formed.
- The failure to generate a chemically active surface due to the ineffective performance or contamination of a surface preparation process during production.

The bonds between the adhesives and the aluminium adherend usually fail since the metallic oxide naturally converts to the hydrated form, causing the original chemical bonds/adhesives to dissociate and cause their separation.

Adhesive bonds that are formed on surfaces and resist to hydration will be durable.

If the failure of adhesion occurs in service, it is due to the manufacturing process. Other commonly advanced causes (displacement stresses due to operational loads, adhesive deformation, or fatigue) can contribute to the final separation of two components that would have eventually failed by some other means. However, they are not the cause of the premature failure by adhesion [10].

The adhesives can be exposed to different mechanical loading conditions. The most common types are shown in Figure 2.3

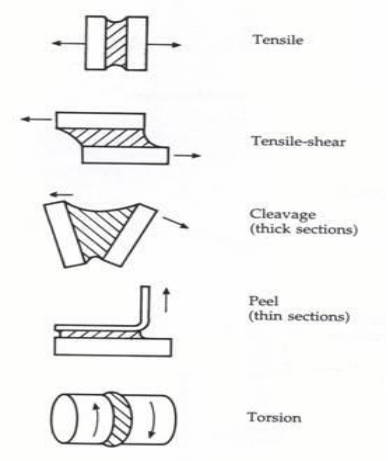


Figure 2.3: Types of stress on adhesive joints[40].

The type of stress depends on how the load is applied, the joint's geometry, and the properties of the adhesive and substrates. The most common joint configuration is the SLJ, the most studied configuration due to its simplicity. Other joint geometries, such as double lap joints, stepped lap joints, and scarf joints, are represented in Figure 2.4 [1].

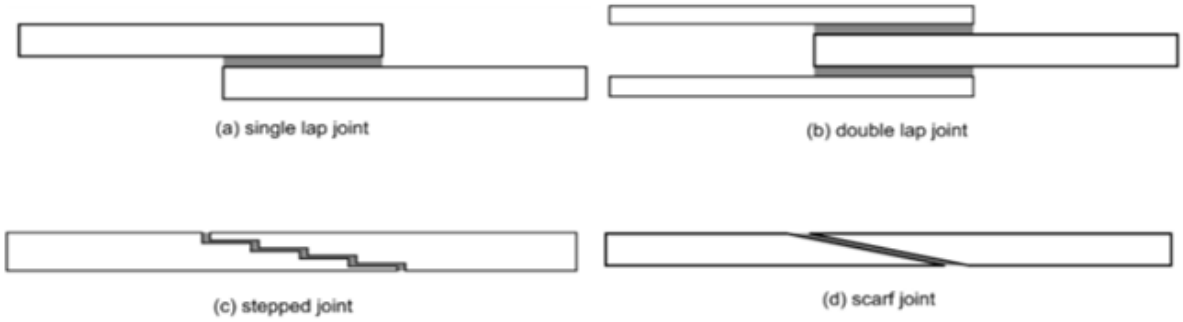


Figure 2.4: Most common joint configurations[41].

## 2.3 Non-destructive tests and evaluation

### 2.3.1 Historical perspective

NDT has been practiced for many decades. These tests have several applications nowadays, but they were initially used to detect surface cracks in the wheels and axles of wagons. The pieces were dipped in oil, then cleaned and sprinkled with powder. When a crack was present, the oil leaked from the defect and wetted the powder, giving a visual indication that the component was damaged. This technique, known as the Penetrant Test, has triggered the creation of several specialized oils for component submerging [12].

X-rays were discovered in 1895 by Welhelm Conrad Roentgen, who was a professor at the University of Würzburg in Germany. Soon after his discovery, Roentgen produced the first industrial radiography. Other electronic inspection techniques, such as ultrasonic and eddy current testing, began with the rapid early development in instrumentation, spurred by technological advances and subsequent defence and space efforts after World War II. Initially, the main objective was to detect defects. Critical parts were produced with a *safe life* design and were designed to work in pristine conditions. The detection of damage was automatically a cause for removing the component from service [12].

NDT started in Shimadzu as part of the "medical division". The Shimadzu Corporation made history in 1909 when it developed the first commercial application of a medical X-ray device. This enterprise has consistently acted as a pioneer in the development of X-ray technology in Japan and abroad, taking advantage of its accumulated knowledge to become one of Japan's leading manufacturers, not only in the medical field but also in a variety of industrial areas. The industrial X-ray device "WELTES" was developed using X-ray technology grown in medical equipment and was launched commercially in 1933. At that time, the need for NDT of steel tube welds in factories arose. Customers were waiting for an industrial X-ray device strong enough to penetrate steel plates, so "WELTES" was released. Subsequently, a fluoroscopic X-ray system with an image amplifier was launched in 1962, and a system for electronic devices was launched in 1984. Shimadzu was successful in developing the first CT X-ray system in 1999 and, since then, came to be considered the leading manufacturer of NDT in Japan [11].

In the early 1970s, an event occurred that caused a significant change in the way inspections were viewed. The improvement of inspection technology, particularly the ability to detect increasingly small failures, has led to the rejection of an increasing number of components. At that time, the field of fracture mechanics rose, which allowed predicting whether a given crack size would fail under a specific load where material properties and fracture toughness were known. Laws were developed to predict the growth rate of cracks under fatigue. Hence, it became possible to accept damaged elements, as long as their defects were tolerable for mechanical performance. This formed the basis for a new design philosophy called *damage tolerant designs*. As such, defective components can still be used if the crack does not reach a critical size. If this critical size is reached, catastrophic failure may occur [12].

A new challenge was then presented to the NDT community. A mere fault detection was not enough, it was also necessary to obtain quantitative information on the size of the fault to serve as an input for fracture mechanics calculations to predict the remaining life of a

component. These needs have led to the creation of several research programs worldwide and NDT's emergence as a new discipline [12].

The SHM started then to appear, providing a continuous evaluation of the structure, and providing more accurate and complete information regarding its state. In order to obtain this information, PZT sensors were commonly used. These sensors were attached to the structure, providing continuous data during its working hours.

### 2.3.2 NDT methods

The NDT is a broad group of analysis techniques widely used in engineering to evaluate a material, component, or system's properties without damaging it. NDT is commonly used in several fields, such as forensic, mechanical, petroleum, electrical, and civil engineering.
Since NDT does not permanently alter the inspected object after the test performance, one can save money and time in maintenance, product evaluation, and research [12, 13].

The six most frequently used methods are:

- Visual and optical testing (VT)
- Penetrant liquid inspection (LPI)
- Magnetic particle inspection (MPI)
- Electromagnetic testing (ET) or eddy current testing
- Radiography (RT)
- Ultrasonic testing (UT)

NDT methods required the use of electromagnetic radiation, sound, and other signal conversions to examine a wide variety of parts regarding their integrity, composition, or condition without destroying or altering it.
Analysing and documenting a non-destructive failure mode can also be performed using a high-speed camera continuously recording until the failure is detected. This failure can be detected using a sound detector or a stress meter that produces a signal to trigger the high-speed camera. After the failure, the high-speed camera will stop recording. The captured images can be reproduced in slow motion showing what happened before, during, and after the non-destructive event [14].

#### 2.3.2.1 Visual and optical testing (VT)

Visual inspection is a NDT method where one merely uses an inspector’s vision to look for possible defects. Specialized tools such as magnifying glasses, mirrors, or borescopes can also be used to gain access and more closely inspect the area in question [13].

#### 2.3.2.2 Penetrating liquid inspection (LPI)

Penetrating liquid inspection is a method to reveal surface cracks by bleeding a coloured or fluorescent dye from the defect. This technique is based on a liquid's ability to be drawn to a *clean* surface breaking flaw by capillary action (Figure 2.5). Pasted the time called *dwell*, the excess penetrant from the surface is removed, and a developer is applied, acting as a blotter (Figure 2.6). It removes the penetrant from the fault to reveal its presence. Coloured penetrants require good white light, whereas fluorescent penetrants require dark conditions with an ultraviolet *black light* [12,15].

The advantage of LPI over VT is that LPI makes defects easily detectable. It produces a fault inspection that is easier to detect with the eye, and the high level of contrast between the indication and the background also helps to make the indication more easily noticeable [12]. When a fluorescent penetrant inspection is made, the penetrating materials are formulated to shine brightly and emit light at a wavelength to which the eye is most sensitive in low light conditions, as shown in Figure 2.7 [12].

This non-destructive assessment is one of the most used due to its flexibility and ease of use. Almost any material can be inspected by LPI, with the proviso that its surface is not overly rough or porous. The LPI materials usually inspected are metals, glass, ceramics, rubbers, and plastics [12].

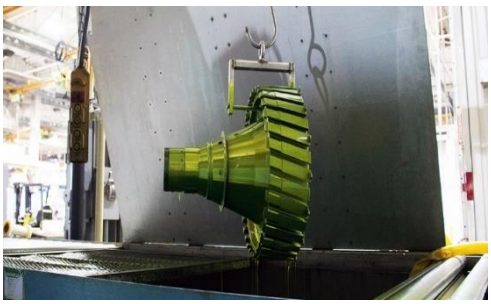

Figure 2.5: Liquid applied to the surface of the part.

Figure 2.6: Removal of the excess liquid from the surface.

The LPI is used to inspect the flaws that break the sample's surface, such as fatigue cracks, grinding cracks, quench cracks, overload, impact fractures, and porosity [12].

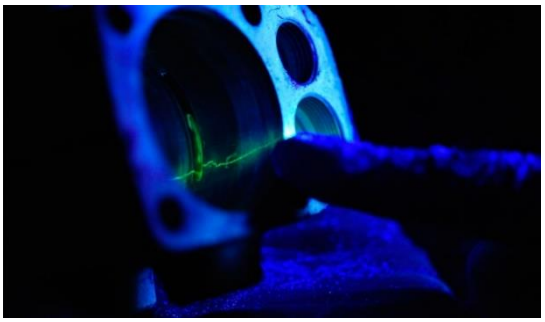

Figure 2.7: Visual inspection under UV light.

One of the main advantages of this process is its high sensitivity to small surface discontinuities. There are minimal limitations on the range of materials that can be tested; metallic, non-magnetic, and conductive and non-conductive materials may be inspected. Large areas and volumes can be inspected quickly and at a low cost. Parts with complex geometric shapes are another example of the applicability of this process [15].

Indications are produced directly on the surface part and constitute a visual representation of the defect, and the aerosol spray cans make the penetrating materials very portable. The cost of the penetrating materials and associated equipment is relatively low.

LPI's main disadvantages are that only surface break defects can be detected, and only materials with a relatively non-porous surface can be inspected. The finish and roughness of the surface can affect the inspection sensitivity. If the part is not very clean, contaminants can mask the defects. Also, metal smearing from machining, grinding, and grit must be removed before LPI [15].

The inspector must have direct access to the surface being analysed. Multiple process operations must be performed and controlled. Chemical handling and proper disposal are required [12].

#### 2.3.2.3 Magnetic particles test (MPI)

Inspection by magnetic particles is another NDT used for defect detection. This method is quick and relatively easy to perform, and unlike other NDT methods, it does not require careful surface preparation. As such, MPI is also one of the most widely used NDT methods.

MPI tests use magnetic fields and small magnetic particles to detect component failures, so the only requirement is that the inspected component must be ferromagnetic, such as iron, nickel, cobalt, or some of their alloys [12].

In theory, the MPI method can be considered a combination of two NDT: magnetic leakage and visual tests.

Consider the case of a magnetic bar (Figure 2.8). The magnetic bar produces a magnetic field in and around the magnet. Any place where a line of magnetic force leaves or enters the magnet is called a pole. The pole where the magnetic field leaves is called the north pole and the pole where a force line enters the magnet is called the south pole.

When a magnetic bar is broken at the centre of its length, it results in two magnetic bars with magnetic poles at each piece's end. If the magnet is only cracked and not completely broken in two, a north pole and a south pole will form on each crack's edge [12].

The magnetic field spreads when it encounters a small amount of air since it owns a smaller magnetic permeability than a magnet. The spreading of the field can be analogously

viewed as a leak in a container, and, as such, it is called a flow leak. If the iron particles are sprayed on a cracked magnet, the particles will be attracted and grouped not only at the poles at the ends of the magnet, but also the poles at the edges of the crack. This particleboard is much easier to see than the actual crack, being this the basis for the inspection of magnetic particles. It is essential to realize the orientation between the magnetic force lines and the failure to properly inspect a component for cracks or other defects [12].

Two general types of magnetic fields can be established within a component: longitudinal magnetic field and circular magnetic field, as seen in Figures 2.10 and 2.11.

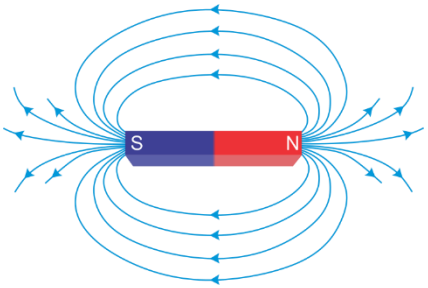


Figure 2.8: A bar with 2 poles [42].

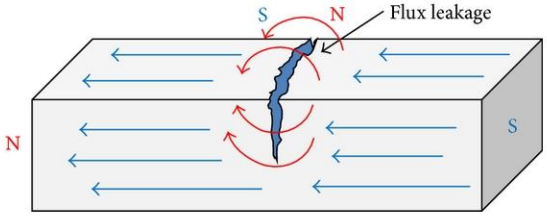


Figure 2.9: Flux leakage field [43].

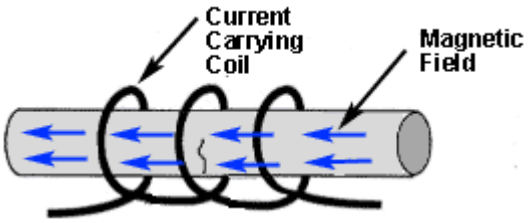


Figure 2.10: Longitudinal magnetic field [45].

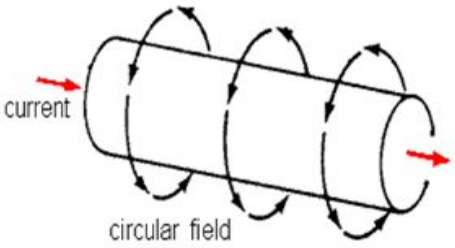


Figure 2.11: Circular magnetic field [44].

The type of magnetic field established is determined by the method used to magnetize the sample. One must be able to magnetize the part in two directions since the best defect detection occurs when the magnetic force lines are established at right angles to the largest dimension of the defect. This orientation creates the most significant disruption of the magnetic field within the part and the most significant leakage of flux on the part's surface. If the magnetic field is parallel to the defect, the field will suffer little interruption, and no flow leakage field will be produced. A 45 to 90-degree orientation between the magnetic field and the defect is required to form an indication (Figure 2.12). Since defects can occur in several directions, each part is generally magnetized in two directions at the right angles. Considering Figure 2.9, it is known that the magnetic field passing through the end to end will establish a circular magnetic field that will be 90 degrees with the direction of the current, as shown in Figure 2.10. Therefore, defects with a significant dimension in the direction of the magnetic

flux (longitudinal defects) must be detectable. Defects of the transverse type will not be detectable with circular magnetization (Figure 2.13) [12].

To properly inspect a part for defects, it is essential to be familiar with the different magnetic fields and equipment used to generate them. To properly inspect a component, it is vital to establish a magnetic field in at least two directions. There are several devices to establish the magnetic field for MPI. One way to classify the device is its portability.

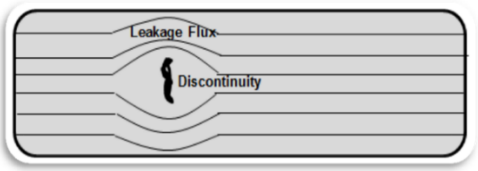


Figure 2.12: The importance of magnetic field orientation [44].

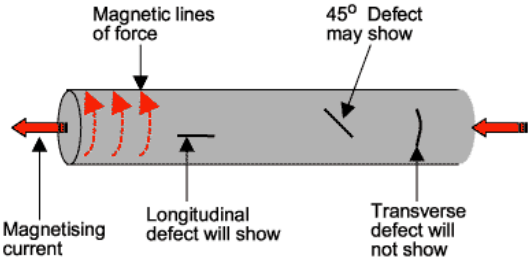


Figure 2.13: Detectability of flaws according to direction of magnetic field [46].

Some equipment is designed to be portable, such as permanent magnets, electromagnets, prods, portable coils, conductive cables, and portable power supplies so that inspections can be carried out in the field. Others are designed to be stationary as it helps inspections in the laboratory or factory. The inspection of magnetic particles can be performed using particles that are quite visible under white light conditions or UV light conditions (Figure 2.14) [12].

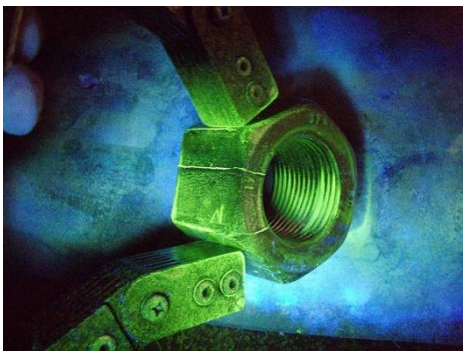

Figure 2.14: Lights for magnetic particle inspection.

#### 2.3.2.4 Electromagnetic testing (ET) or eddy current testing

Electric currents are created in a conductive material by an induced alternating magnetic field. Interruptions in the flow of eddy currents, caused by imperfections, dimensional changes, or the material's conductivity and permeability properties can be detected with the appropriate equipment [15].

The process, called electromagnetic induction, creates eddy currents. When alternating current is applied to the conductor, such as a copper wire, a magnetic field develops inside and around the conductor. This magnetic field expands when the alternating current reaches its maximum value and collapses when the current reaches zero. If another electrical conductor is brought close to this variable magnetic field, the current will be induced in this second conductor. Eddy currents are the induced electrical currents that flow in a circular path. They are called *whirlpools* formed when a liquid or gas flows in a circular path around an obstacle, as can be seen in Figure 2.15 [12].

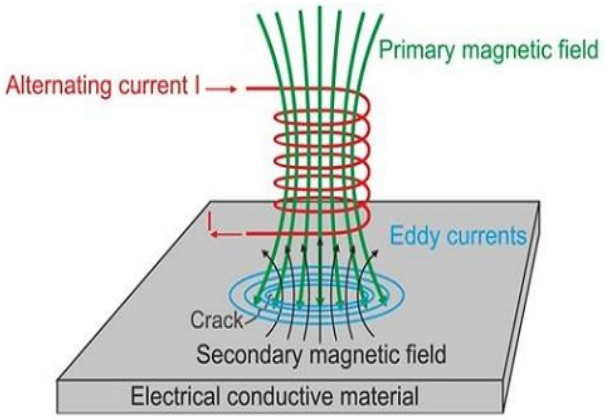


Figure 2.15: Eddy current principle [47].

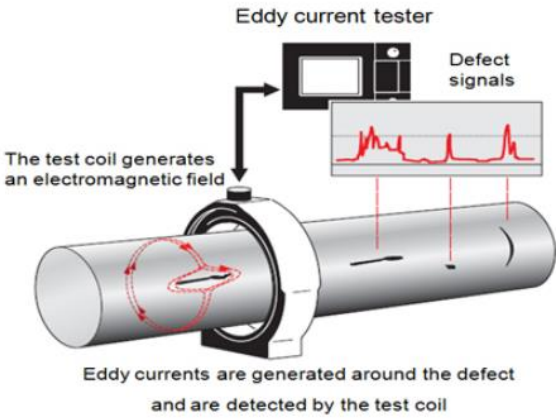


Figure 2.16: A test coin scanning over the part surface in an attempt to detect a crack [13].

One of the main advantages of eddy current as an NDT tool is the variety of inspections and measurements that can be performed. In certain circumstances, eddy currents can be used for crack detection (Figure 2.16), material thickness measurements, coating thickness measurements, and conductivity measurements. Conductivity measurements can have several uses, such as material identification, heat damage detection, box depth determination, and heat treatment monitoring. Its sensitivity to small cracks and other defects is one of the main advantages of this method. The inspection gives immediate results and uses very portable equipment. However, the part needs minimal preparation [12,16].

The limitation of conductive materials and the accessibility of the surface are the main disadvantages of this method. The training required by NDT technicians to perform eddy-current testing is more complicated than other techniques. Surface finish and roughness can interfere. The penetration depth is limited, and faults such as delamination parallel to the probe coil's winding and the probe's scan direction are undetectable [12,16].

#### 2.3.2.5 Radiography

This method involves the use of penetrating gamma or X radiation to examine parts and products for imperfections. An X-ray generator or radioactive isotope is used as a radiation source. Radiation is directed through a part and onto film or other imaging media. The resulting shadowgraph shows the dimensional features of the part. Just as a medical X-ray shows broken bones, possible imperfections can be detected as density changes in the film [12,15].

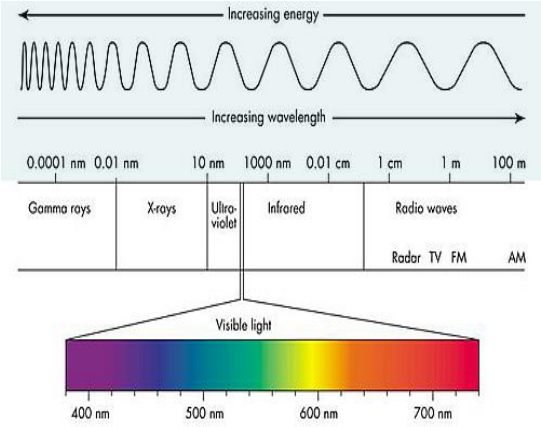


Figure 2.17: The electromagnetic spectrum.

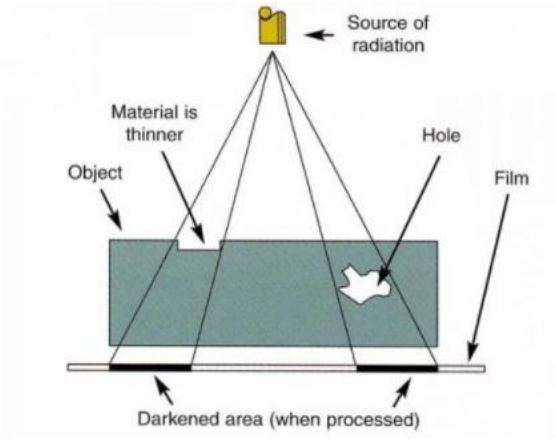


Figure 2.18: Radiography methodology to detect damage [13].

When X-rays or gamma-rays are directed at an object, some photons interact with the particles of matter, the energy can be absorbed or spread, and this absorption and dispersion is called attenuation. Other photons travel through the object without interacting with any of the particles in the material. The number of photons a material transmits depends on the thickness, density, atomic number, and photon's individual energy. Even when the transmitted photons have the same energy, photons travel different distances within a material based on the likelihood of encountering one or more of the atomic particles and the type of encounter that occurs. The probability of an encounter increases with the covered distance, the number of photons that reach a specific point within the matter decreases exponentially according to the distance covered [12].

The formula that describes this curve is

$$I = I_0 e^{-\mu x} \tag{2.1}$$

where $I$ is the intensity of the photons transmitted over some distance $x$, $I_0$ is the photons' initial intensity, and $\mu$ is the linear attenuation coefficient [12].

The constant $\mu$ is the factor that indicates how much attenuation will occur per length unit and describes the fraction of X-ray or gamma-ray beam absorbed or spread per unit of the absorber's thickness. When the incident X-ray photon is diverted from its original path due to an interaction with an electron, scattering occurs. The electron is ejected from its orbital position, and the X-ray photon loses energy due to the interaction but continues to travel through the material along an altered path. In this process, energy and momentum are conserved and is called Compton effect [17].

The change in energy does not depend on the mirroring medium's nature but rather on the mirroring angle. Compared to the incident photon, the energy photon has less energy, a longer wavelength, and less penetration [12].

The change in wavelength of the scattered photon is given by [12]

$$\lambda' - \lambda = \frac{h}{m_e * c}(1 - \cos\theta) \tag{2.2}$$

where:

- $\lambda$ is the wavelength of incident X-ray photon
- $\lambda'$ is the wavelength of scattered X-ray photon
- $h$ is the Planck's Constant ($h = 6.63 * 10^{-34}$ J/s)
- $m_e$ is the mass of an electron
- $c$ is the speed of light
- $\theta$ is the scattering angle of the scattered photon.

The interpretation of radiographic films is an acquired skill that combines visual acuity with knowledge of materials, manufacturing processes, and the associated discontinuities. If the component is inspected during service, it is essential to understand the loads applied to it and its history. A radiographic visualization process is essential and will avoid neglecting an area on the radiograph [12].

This process is often developed over time and individualized. Both eyes and minds occasionally need to rest when interpreting radiographs. Techniques such as using a small light source, moving the X-ray over the small light source, changing the light source's intensity, or changing the light will help the radiology technician identify relevant information [12].

Magnification tools should also be used to help identify and evaluate indications. Viewing the actual component being inspected is often important to understand the details seen on a radiograph. The interpretation of radiographs is improved over time, using appropriate equipment, and developing consistent assessment processes. The interpreter will increase the chance of detecting defects [12].

Compared to other NDT techniques, radiography has many advantages. It is highly reproducible, can be used on various materials, and the data gathered can be stored for later analysis. Radiography is a useful tool that requires very little surface preparation. Furthermore, many radiographic systems are portable, which allows for use in the field and at elevated positions [15].

Radiography is often used in the petrochemical industry to inspect machinery pieces, such as pressure vessels and valves, and to detect flaws. It is also used to inspect weld repairs [15].

#### 2.3.2.6 Ultrasonic test (UT)

Ultrasonic tests use the high-frequency sound wave transmission in material to detect imperfections or locate changes in the material properties. The ultrasonic test most commonly used is pulse echo, where the sound is introduced into a test object, and the reflections (echoes) return to a receiver from internal imperfections or the geometrical surfaces of the part [12,18].

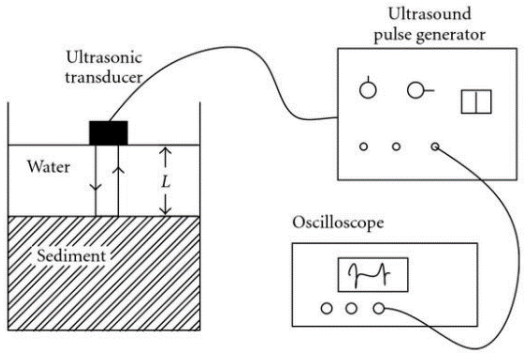


Figure 2.19: Typical ultrasonic system [48].

A typical UT inspection system consists of several functional units, such as the pulsator/receiver, transducer, and display devices (Figure 2.19). An electronic device capable of producing high voltage electrical pulses is called a pulsator/receiver. The transducer generates high-frequency ultrasonic energy, driven by the pulsator. The sound energy is supplied and propagates through the materials in the form of waves. When there are discontinuities (a crack or void) in the wave path, part of the energy will be reflected from the defect surface. The reflected wave signal is transformed into an electrical signal by the transducer and is displayed on the screen. The signal travel time can be directly related to the distance the signal has travelled. Sometimes, it is possible to obtain information about the location, size, orientation, and other reflector features [12,18].

In solid media, sound waves can propagate in four main ways based on how the particles oscillate. The sound can propagate as shear waves, longitudinal waves, surface waves, and thin

materials like plate waves (Figure 2.20). The two most widely used modes of propagation in ultrasonic testing are longitudinal and shear waves [12].

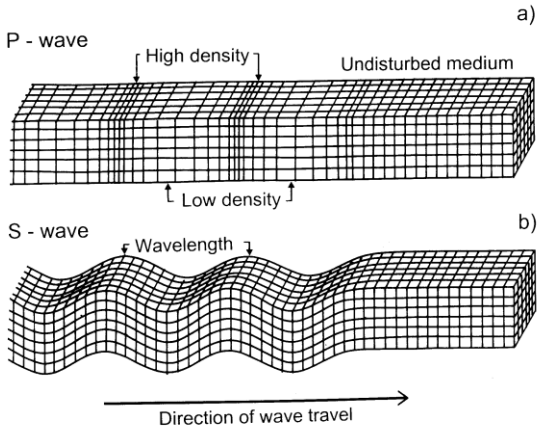


Figure 2.20: Longitudinal and shear waves [49].

When performing a given UT, one must first define a given wave frequency. Changing the frequency, when the sound's speed is fixed, causes the wavelength to change. The wavelength of the soundwave used has a significant effect on the probability of detecting discontinuity. In general, for a discontinuity to have a chance of being detected, its size must be greater than half the wavelength.

The intensity of the sound decreases with distance when it travels through a medium. When sound waves pass through an interface between materials each with acoustic speeds, wave refraction will occur at the interface. The fraction of incident wave that is refracted at the interface is proportional to the difference in acoustic velocity. This effect is less noticeable in shear waves since the shear waves are slower than the longitudinal waves. It is also observed that when a longitudinal wave is reflected within the material, the reflected shear wave is reflected at a smaller angle when compared to the reflected longitudinal wave. This event is also because the sheer speed is less than the longitudinal speed within a given material [12]. This phenomenon is explained by Snell's law shown in Figure 2.21.

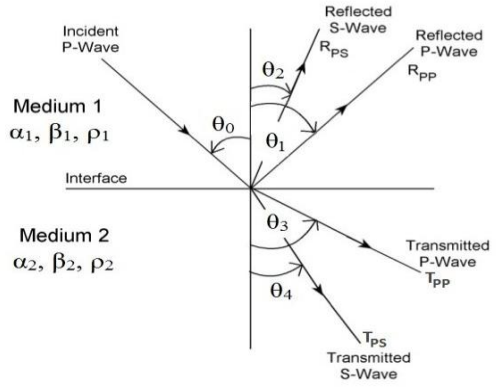


Figure 2.21: Snell's law [50].

Snell's law is given by,

$$\frac{\sin\theta_1}{V_{L1}} = \frac{\sin\theta_2}{V_{L2}} = \frac{\sin\theta_3}{V_{S1}} = \frac{\sin\theta_4}{V_{S2}} \tag{2.3}$$

where:

-$V_{L1}$ is the longitudinal wave velocity in material 1

- $V_{L2}$ is the longitudinal wave velocity in material 2

-$V_{S1}$ is the shear wave velocity in material 1

-$V_{S2}$ is the shear wave velocity in material 2

An angle of incidence makes the longitudinal wave's refractive angle 90 degrees when a wave moves from a slower material to a faster one. This is known as the first critical angle, and all the energy of the refracted longitudinal wave is converted to a surface after the longitudinal wave. After the surface, this wave is sometimes called a creep wave and is not very useful in NDT because it dampens very quickly. In addition to the first critical angle, only the shear wave propagates to the material.

As such, usually, ultrasound NDT is performed with shear waves, thus, avoiding the issue of having to process two waves. Often there is also an angle of incidence that makes the angle of refraction for the shear wave 90 degrees. This feature is known as the second critical angle, at which point all wave energy is reflected or refracted on a surface after the shear or shear creep wave. The surface waves will be generated just beyond the second critical angle.

Ultrasonic inspection is an advantageous and versatile NDT method. Sensitivity to surface discontinuities and the depth of penetration for damage detection and measurement are advantages of ultrasonic inspection when compared with other NDT methods. Only single-sided access is needed when the pulse-echo technique is used. It is highly accurate to estimate the size and shape and determine the position of the damage. Minimal preparation of the part is required. Electronic equipment provides instantaneous results. Detailed images can be produced with automated systems [12,18].

Besides damage detection, the UT is able to perform thickness measurement. This method also has its disadvantages, including skill and more extensive training than with some other methods. The surface must be accessible to transmit ultrasound. Generally, it requires a coupling means to promote the transfer of sound energy to the specimen. Materials that are rough, irregularly shaped, very small, or inhomogeneous are challenging to inspect. Among these materials are cast iron and other coarse-grained materials due to low sound transmission and high signal noise. Furthermore, linear defects oriented parallel to the sound beam may not be detected [12,15].

## 2.4 Lamb waves

Horace Lamb, in 1917, discovered LW [19]. LW exist in thin plate-like structural components and are guided by the two parallel free boundaries. LW can also travel inside curved walls with the shallow curvature. LW can propagate to long distances with minor amplitude damping due to the low damping imposed by the free boundaries, even in materials with a high attenuation ratio. It is also interesting to realize that most aircraft structural components can be decomposed into several plates or shells like cross-sections.

In 1961, Worlton [20] suggested the potential of applying LW for structural inspection and damage detection, and a new NDT potential technique emerged. The fascinating behaviour of LW is the ability to detect reflections generated by the interference with damages (boundaries and other material or geometry discontinuities).

Essential features that must be considered in the development of an LW-based inspection method are [21]:

- the wave propagation characteristics in the host medium;
- the types of transducers to be used and how they are applied to the structure;
- the actuation type;
- the type of signal processing and evaluation.

Research is being performed in different aspects of this problem. LW generation and propagation behaviour, the transducer's influence on such aspects, and the application of numerical methods and experimentation were previously investigated [22].

LW experiments in aluminium plates proved that these high frequency waves were sensitive to damage, mainly when the distance between the damage and the wave's direct path was short [23].

Damage prognostic systems and failure prediction techniques have recently been the subject of demanding research and development in a broad range of engineering applications. The use of LW due to its facility of detecting internal damage as well as that on the surface is considered one of the most effective NDT used by aeronautic structures.

LW present stationary patterns across the material thickness, featuring two fundamental modes: symmetric and asymmetric (and, respectively, where represents the number of inflection points across the material thickness), as shown in Figure 2.22 [24].

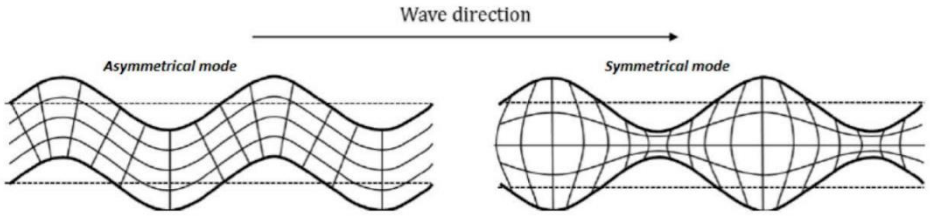


Figure 2.22: First symmetric (S0) and anti-symmetric (A0) Lamb wave modes [51].

As the name indicates, asymmetrical LW also known as flexural or shear waves will cause the material particles to oscillate asymmetrically about the middle plane ($A_n$). These waves oscillate perpendicularly compared to the direction of the waves propagation as shown in Figure 2.23

On the contrary, the symmetrical waves (*Sn*, also called extensional waves) travel symmetrically through the middle plane of the plate, being known as pressure waves, once the particle motion and the direction of the wave propagation match as shown in Figure 2.23. Therefore, waves are most efficiently produced when the exciting force is parallel to the plate and waves when the exciting force is perpendicular to the plane.

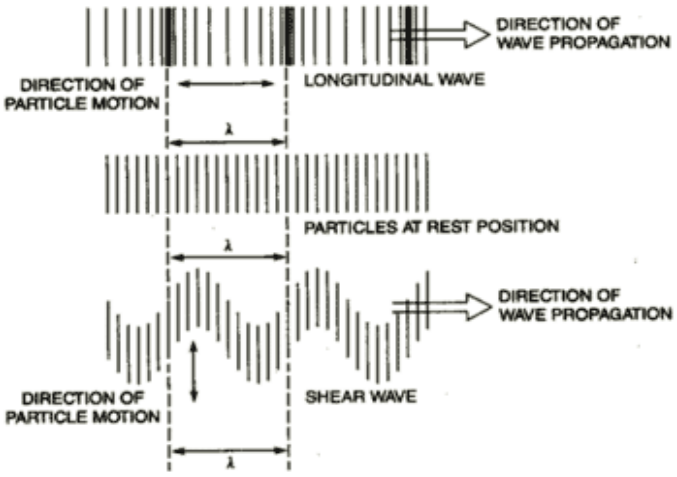


Figure 2.23: Direction of particle motion of symmetric and asymmetric modes in comparison with de direction of the wave propagation [12].

Another significant characteristic of LW is their dispersive behaviour dependence of propagation velocity to their frequency [25].

Piezoelectric transducers have been selected in most cases to generate LW [26]. They can work at high frequencies, both as actuators and sensors. Their size, shape, and location must be carefully chosen [27].

### 2.4.1 Dispersion curves

As referred previously, LW modes are typically dispersive. As such, phase and group velocity depend on frequency for a given sample.

Dispersion curves are of paramount significance in selecting the actuation signal, the transducers to be applied, their material, and size. If multiple excitation frequencies are applied in wave generation, groups of waves with different propagation velocities will be generated in terms of actuation. The latter introduces noise and added complexity in wave propagation patterns as on their evaluation. The selection of an actuation signal centred in a single frequency is then recommended [28].

Moreover, for higher actuation frequencies, secondary modes may be excited. In this case, the generated waves will be a combination of different modes with different propagation velocities and deformation patterns, raising once more the complexity in the analysis of sensors' signals. Through the observation of dispersion curves, a frequency range for actuation can be established to prevent the excitation of multiple modes. Also, a difference in $S_0$ and $A_0$ propagation velocities is advantageous, since their corresponding sensed signals would be well separated in time [28].

The LW group velocity ($C_g$) represents the speed with which LW packs are sent and received along with the thin-wall plate. The product between frequency and the material thickness ($h$) gives the LW phase velocity ($C_L$) [29].

To calculate the shear waves velocity ($C_s$) and phase waves velocity ($C_p$) one resorts to the Young modulus($E$), density ($\rho$) and Poisson ratio ($\nu$) of the propagation medium as shown in equations (2.4) and (2.5):

$$C_s = \sqrt{\frac{E}{2\rho(1+\nu)}} \tag{2.4}$$

$$C_p = \sqrt{\frac{\nu E}{(1+\nu)(1-2\nu)\rho} + \frac{E}{\rho(1+\nu)}} \tag{2.5}$$

Having calculated (2.4) and (2.5) it is possible to obtain the dispersion curves by solving the Rayleigh-Lamb frequency equation. This equation varies due to the mode, in which $d$ is the half-thickness of the plate, and $w$ the angular frequency. For the symmetric mode the equation is:

$$\frac{\tan\sqrt{1-\zeta^2}\bar{d}}{\tan\sqrt{\xi^2-\zeta^2}} + \frac{4\zeta^2\sqrt{1-\zeta^2}\sqrt{\xi^2-\zeta^2}}{(2\zeta^2-1)^2} = 0 \tag{2.6}$$

Being the two components of displacement:

$$U(x,y,z) = Re\left[Ak_L\left(\frac{\cosh(qz)}{\sinh(qd)} - \frac{2qs}{k_L^2+s^2}\frac{\cosh(sz)}{\sinh(sd)}e^{i\left(k_Lx-wt\frac{\pi}{2}\right)}\right)\right] \quad (2.7)$$

$$W(x,y,z) = Re\left[Aq\left(\frac{\sinh(qz)}{\sinh(qd)} - \frac{2k_L^2}{k_L^2+s^2}\frac{\cosh(sz)}{\sinh(sd)}e^{i(k_Lx-wt)}\right)\right] \quad (2.8)$$

For the asymmetrical mode the equation is

$$\frac{tan\sqrt{1-\zeta^2}\bar{d}}{tan\sqrt{\xi^2-\zeta^2}} + \frac{(2\zeta^2-1)^2}{4\zeta^2\sqrt{1-\zeta^2}\sqrt{\xi^2-\zeta^2}} = 0 \quad (2.9)$$

And the two components of displacement are

$$U(x,y,t) = Re\left[Ak_L\left(\frac{\cosh(qz)}{\sinh(qd)} - \frac{2qs}{k_L^2+s^2}\frac{\cosh(sz)}{\sinh(sd)}e^{i(k_Lx-wt\frac{\pi}{2})}\right)\right] \quad (2.10)$$

$$W(x,y,t) = Re\left[Aq\left(\frac{\sinh(qz)}{\sinh(qd)} - \frac{2k_L^2}{k_L^2+s^2}\frac{\cosh(sz)}{\sinh(sd)}e^{i(k_Lx-wt)}\right)\right] \quad (2.11)$$

where $\zeta$, $\xi$ and $\bar{d}$ are the lame constants given by:

$$\xi = \sqrt{\frac{c_s^2}{c_p^2}} \quad \zeta = \sqrt{\frac{c_s^2}{c_L^2}} \quad \bar{d} = \frac{2\pi.f.d}{c_s} \quad (2.12)$$

One can also calculate the group velocity $c_g$ by the following equation:

$$C_g = c^2[c - (fd)\frac{dc}{d(fd)}]^{-1} \quad (2.13)$$

where $C_g$ is the LW group velocity, and c is the LW phase velocity.

Equation (2.6) and equation (2.9) admits several roots, corresponding to many symmetrical modes.

The roots of the equation were found numerically using the *SOFTWARE: Dispersion Calculator*, once there is no analytical solution for the equations (2.6) and (2.9). Figures 3.4 and 3.5 show the dispersion curves for LW in a 2 mm aluminium alloy plate. Through the analysis of the figures, one concludes that at low frequencies (f < 500 kHz), the symmetrical

speed LW approaches the speed of axial waves, $C_p$, and at high frequencies (2500 kHz), the dispersion curves for the $S_0$ and $A_0$ modes coalesce.

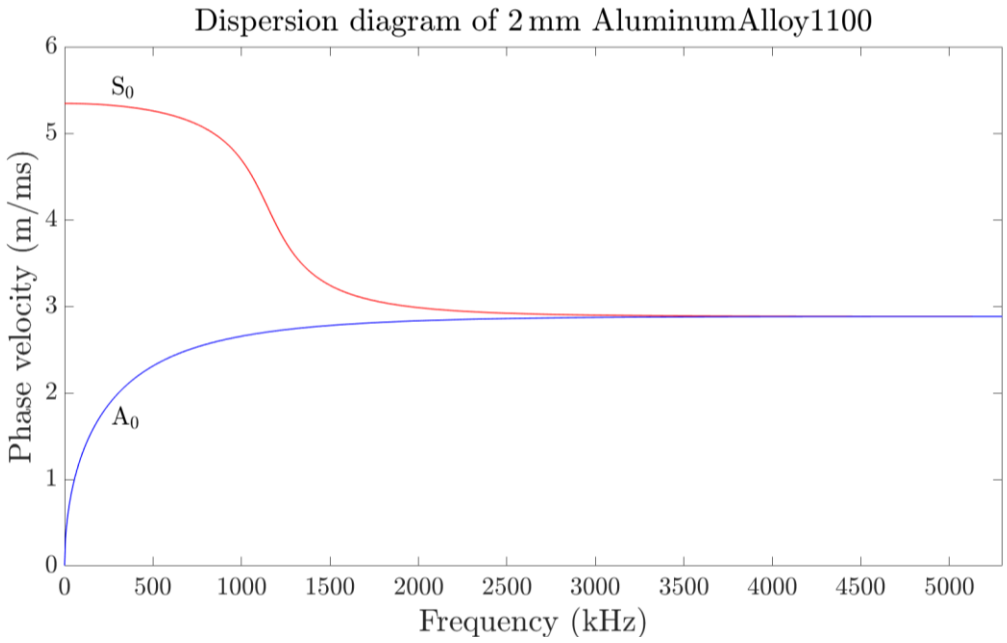


Figure 2.24: Graph of the first two different modes in a 2 mm aluminium plate, phase velocity vs frequency.

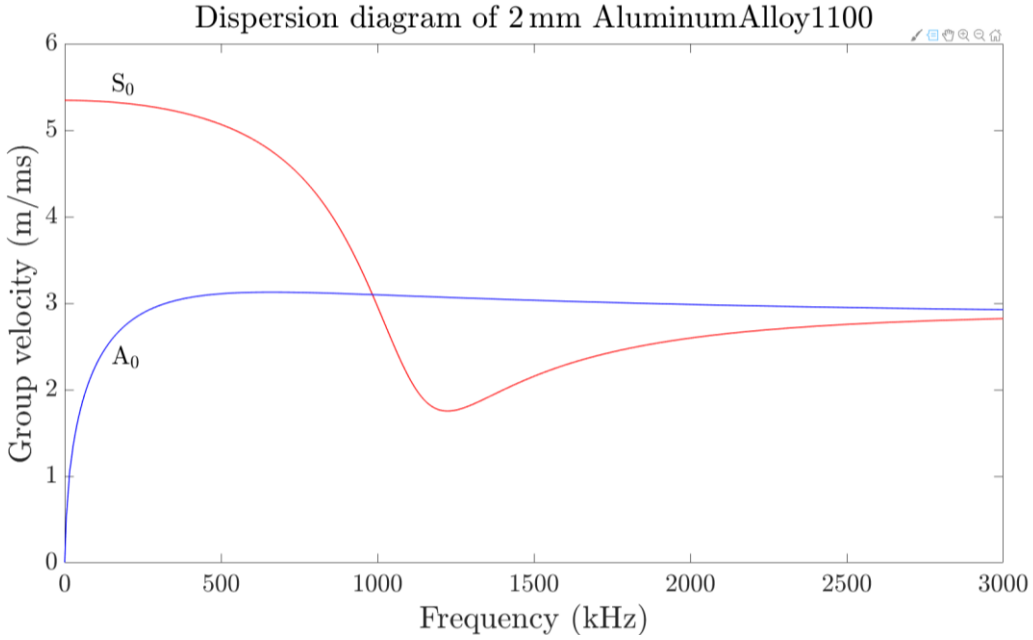


Figure 2.25: Graph of the first two different modes in a 2 mm aluminium plate, group velocity vs frequency.

### 2.4.2 Damage detection

Structural defects represent changes in effective thickness and local material properties, and therefore, variations in LW can be used to examine structures' integrity.

The principle to locate damage is then straightforward. Suppose multiple sensors spread across different locations are used to detect the originally generated LW and their reflections. Knowing their velocity of propagation and the coordinates of the sensors, by triangulation, is

possible to detect their source location, i.e., the damage. This method is known as time of flight diffraction, or difference, or delay (TOFD). After obtaining the sensors signals and analysing them, the problem may be solved by a series of different proposed methods, such as Fourier transforms and numerical methods, expanding potentials to not also detect the damage but also to measure it and locate it [29].

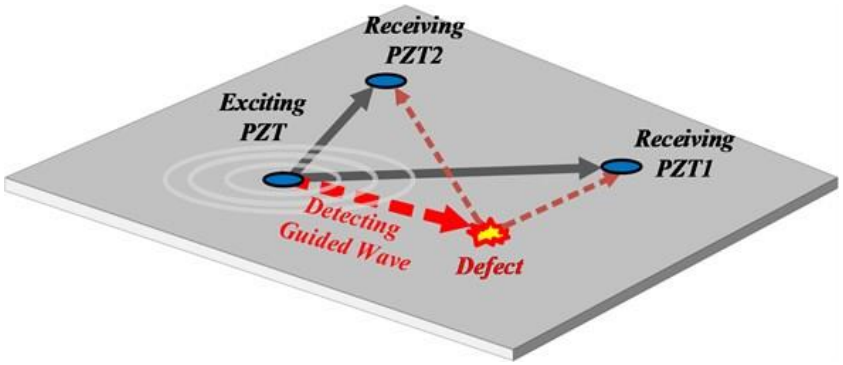


Figure 2.26: Representation of how PZT receive the waves from the damage.

The two different first modes of LW, $S_0$ and $A_0$, can detect different damage types. Cuts imitating cracks are detectable using symmetrical LW modes, while surface damages affect mainly the antisymmetric mode of LW propagation [30]. Besides, the amplitude of reflected waves is proportional to the damage dimension and dependent on damage orientation.

The LW mode used in SHM methods is also highly dependent on the structural configuration to inspect. For instance, if the structure possesses a stiffener, this component will attenuate LW propagation, decreasing their energy and amplitude while generating strong reflections. At least, reflections are one magnitude lower than original incident LW, which possess very low energy and amplitude [29].

This fact makes the task of detecting a reflection challenging. Together with the existence of a stiffener and the implications before mentioned, one may conclude that it will be tough to detect a failure beyond the stiffener. In this particular case, knowing that $A_0$ LW has higher energy than $S_0$, they would be the better choice. However, they present the disadvantage that the propagating velocity is dependent on the incident wave frequency [29].

The characteristics of the reflected waves described before, namely high frequency and low elastic deformation energy, make them susceptible to noise interference in sensor readings. The piezoelectric sensors (PZT) are sensitive, and, since the waves they detect have very low energy, it is possible to conclude that noise will significantly impact measurements.

One attenuating factor is that the sensor signal can be filtered since the frequencies of the LW applied in the inspection method are predetermined.

The need to use high-frequency actuation is explained by the high propagation velocities of LW and the fact that, on specific SHM methods, the actuator is also used as a sensor. This way, the actuation signal will be over and will not interfere with reflections [29].

As mentioned earlier, methods analysed in the time domain for damage location depend on wave time of flight calculations, which rely on the propagation velocity of the host structure waves, calculated based on the dispersion curves.

The time of flight (TOF) is very short, and propagation velocities are very high, so any discontinuity of the material, Young's modulus, and/or density variation is problematic when determining damage position.

### 2.4.3 The measurement of the properties of propagating LW

The fundamental problem associated with the quantitative measurement of the characteristics of propagating LW modes is that multiple modes can exist at any given frequency. As a matter of fact, the higher the frequency, the greater the number of modes. The excitation via transducers means that all modes at any particular frequency of excitation are generated, so it is impossible to separate the modes by merely transforming from the time domain to the frequency domain [31].

If the excitation is not "single frequency", dispersion will be present, leading to complicated time-domain signals. Therefore, the history of the response time of the model would be multimode and dispersive. Thus, the input signal generated needs to excite only low modes, which can be achieved using a Hanning window, as discussed further [31].

Conventional time domain methods of measuring LW amplitudes and velocities generally require minimal signal processing and are often the easiest to apply. Although, if the time history of a wave packet consists of a single mode, it can be resolved separately from other wave packets in the time domain. Its amplitude may be measured, and its group velocity may also be determined by measuring the time it takes to propagate between two known positions [31].

Time-domain techniques may be adapted to measure the amplitude and velocities of $A_0$ and $S_0$ in low frequency-thickness regions where there are only two propagating modes. Since their phase velocities are very different, they may be easily identified. When the time record is composed of several superimposed wave packets, it is usually impossible to measure individual LW amplitude or group velocity. Hence, many researchers have used time-domain correlation methods [35, 36]. In 1983, a method using a similarity coefficient was developed, where the spectrum of received signals is compared with a reference or a good spectrum [31].

However, none of these methods have obtained reliable results at frequency above the cut-off value for the respective $A_1$mode.

Other methods used a reflection coefficient technique to measure leaky LW dispersion curves and determine material properties. However, the LW relative amplitudes cannot be easily identified [31].

The next section will introduce the standard spectral methods of measuring LW velocities when only one mode is present. A two-dimensional Fourier transformation method will also be presented, which can measure the amplitudes and velocities of LW when many propagating modes are present.

#### 2.4.3.1 Frequency domain methods

Early investigations to detect different echoes in seismic signals used a spectrum analysis, a logarithmic conversion of the spectrum of the time record. More recently, spectral methods have been used to measure phase and group velocity by transforming the time domain data to the frequency domain, where data interpretation may be more accessible. To measure the dispersion curve of a single LW, one may use the Fourier transform of the time record containing a series of echoes from a single position. Alternatively, the time records of model response at two or more known locations may be summed and applied the Fourier transform [31]. The resulting amplitude spectrum will have resonance peaks, from which the phase velocity of the LW at discrete frequencies can be calculated using a relation given as

$$c = \frac{L*F}{n}, n = 1,2 \ldots \tag{2.14}$$

where $L$ is the distance between the measurement positions and $c$ is the LW phase velocity. If we separate the echoes in the time domain, a phase spectrum method can be used. Two-time records or echoes are Fourier transformed separately, through the relation given as

$$c = \frac{L\omega}{\Delta\varphi} \tag{2.15}$$

It is used to calculate the phase velocity, where $\Delta\varphi$ is the difference in the phase spectrum of the two signals. The result of carrying out a discrete-time Fourier transform of a time history of the response of the model is that a plot of amplitude versus frequency is obtained. Still, there is no information about which Lamb modes are present [31]. Due to the multimode dispersive nature of LW, the probability of multiple modes being excited by broadband excitation signals,

amplitude, and phase spectrum methods of measuring the dispersion curves is not usually applied frequency-thickness regions above 1.63 MHz.

#### 2.4.3.2 The two-dimensional Fourier transform method

The two-dimensional Fourier transformation method discussed in this section is an extension of the one-dimensional Fourier transformation method developed by Sachse and Pao [37]. It is an alternative method of measuring the properties of LW. It overcomes multiple modes and dispersion problems by transforming the received amplitude-time records to amplitude-wavenumber records at discrete frequencies, where individual LW can be identified, and their amplitudes measured. The significant advantage of this method is that LW amplitudes and velocities are measured, which is of great importance in NDT applications. Propagation distances may be vast and are limited only by the signal-to-noise ratio [31].

#### 2.4.3.3 RAPID (Reconstruction Algorithm for the Probabilistic Inspection of Damage)

The principle behind this method is the quantitative measurement of the differences between the obtained signals from the specimen with and without defect.

The primary assumption is that this difference is related to the presence of the damage. This difference would be most significant if the damage presented itself in the direct path of the wave, and consequently, the influence of the damage would decrease with the distance.

In order to use the RAPID method for the specimen inspection, certain assumptions have to be implemented [32, 33]. Firstly, a damage index should be defined, for instance, the correlation coefficient given by

$$\rho = \frac{cov_{XY}}{\sigma_X \sigma_Y} = \frac{cov(X,Y)}{\sqrt{Var(X)Var(Y)}} \tag{2.16}$$

where $cov_{XY}$ is the covariance of $X$ and $Y$, being X and Y the respective vectors of the signals being analysed. Therefore, the coefficient $\rho$ is rewritten in equation (2.17), where $\bar{X}$, $\bar{Y}$are the variable's average values. In order to locate the damage, it is also assumed that the probability of a defect at an arbitrary point (calculated as damage intensity) could be assessed by the relative position of the sensors' locations and the magnitude of the signal change.

$$\rho = \frac{\sum_{i=1}^{n}(X_i-\bar{X})(Y_i-\bar{Y})}{\sqrt{\sum_{i=1}^{n}(X_i-\bar{X})^2 \cdot \sum_{i=1}^{n}(Y_i-\bar{Y})^2}} \tag{2.17}$$

Due to the assumption that this intensity would decrease with the distance from the direct path, an ellipse is defined, and its intensity progresses according to the equation (2.19), which is valid inside the ellipse area. The damage intensity within the sensor network could thus be calculated as the linear addition of all signal change magnitude results. It is defined by equation (2.18).

$$I(x,y) = \sum_{k=1}^{N_p}(1-\rho_k)\left(\frac{\beta - R(x,y)}{\beta - 1}\right) \tag{2.18}$$

where $N_p$ is the number of paths, $(1-\rho_k)$ is the main factor for the path k and can be replaced by another damage index in Table (2.1). The scaling factor β determines a valid effective area in an elliptical form for a pair of transducers. Hence, the reduction effect of the physical influence is controlled by $\beta$. $R(x,y)$ is defined with the β as:

$$R(x,y) = \begin{cases} \frac{\sqrt{(x-x_i)^2+(y-y_i)^2}+\sqrt{(x-x_j)^2+(y-y_j)^2}}{\sqrt{(x_i-x_j)^2+(y_i-y_j)^2}}, R(x,y) \geq \beta \\ \beta,\ R(x,y) < \beta \end{cases} \tag{2.19}$$

where ($xi$, $yi$) and ($xj$,$yj$) are the pair's positions consisting of transmitter and receiver. The ellipse form, determined by the eccentricity $\varepsilon$, is only dependent on $\beta$ and should be greater than 1 and smaller than 1.2 [34].

$$\varepsilon = \frac{1}{2\beta - 1} < 1,\ \beta > 1 \tag{2.20}$$

The suitable choices of the damage index are studied by [33]. The indices that adequately identify and localize damage are based on

- the maximum amplitude (SAPR: Signal Amplitude Peak Ratio, SAPS: Signal Amplitude Peak Squared Percentage Differences),
- the amplitude over the entire signal (SSSD: Signal Sum of Squared Differences),
- the covariance matrix,

which are listed in Table 2.1. The correlation coefficient mentioned above is also error-sensitive, according to [19].

Table 2.1: Different type of damage indices.

| Method name | Basis | Abbr. | Formula |
|---|---|---|---|
| Correlation Coefficient | Correlation | CC | $\rho = \frac{\sum_{i=1}^{n}(X_i - \bar{X})\,(Y_i - \bar{Y})}{\sqrt{\sum_{i=1}^{n}(X_i - \bar{X})^2 \cdot \sum_{i=1}^{n}(Y_i - \bar{Y})^2}}$ |
| Signal Sum of Squared Difference | Amplitude over the whole signal | SSSD | $DI = \frac{\sum(S_H - S_D)^2}{\sum {S_H}^2}$ |
| Signal Amplitude Peak Squared Percentage Differences | Maximum of amplitude | SAPS | $DI = \left(\frac{(\max[S_H] - \max[S_D])}{\max[S_H]}\right)^2$ |
| Ratio of covariance matrix eigenvalues | Covariance matrix | RCME | $\rho = 1 - \frac{\lambda_2}{\lambda_1}, \qquad \lambda_1 > \lambda_2$ |

In short, to study the condition of adhesives, most of the aforementioned NDT methods would strive. However, given that SLJ are sensitive to heat or humidity (characteristics that may harm the adhesion between the substrate and the adhesive), which may cause the appearance of defects, these NDT techniques may not be the most adequate. As such, the most promising NDT method would be ultrasonic testing. This method, in combination with the use of PZT sensors, is able to perform SHM to the adhesive joint. Therefore, in order to analyse the condition of the SLJ without damaging it, one can resort to LW, because they can detect both surface and internal damage. Given that the propagation of the Lamb Waves resorts to particle displacement, their implementation will not harm the SLJ. Also, given that the adhesive is a material with good attenuation of mechanical vibrations and sound, it is easier to detect defects embedded in the adhesive layer using LW.

With sensor data collected, the ways in which the results can be studied are vast, although, due to the simplicity of obtaining time-domain signals, a comparison of the obtained signals is often used as a first approach to detect a defect. A more complex approach would be to locate

the defect, and in doing so, analysing the signals in the frequency domain. However, for this method, the number of sensors attached to the SLJ would increase.

For these reasons, these are the techniques that will be addressed in chapters 3 and 4.

# 3 Experimental procedure

## 3.1 Set-up

The experimental set-up comprises a computer, a function generator, an oscilloscope and SLJs, with and without defects, instrumented with piezoelectric sensors (Figure 3.1).

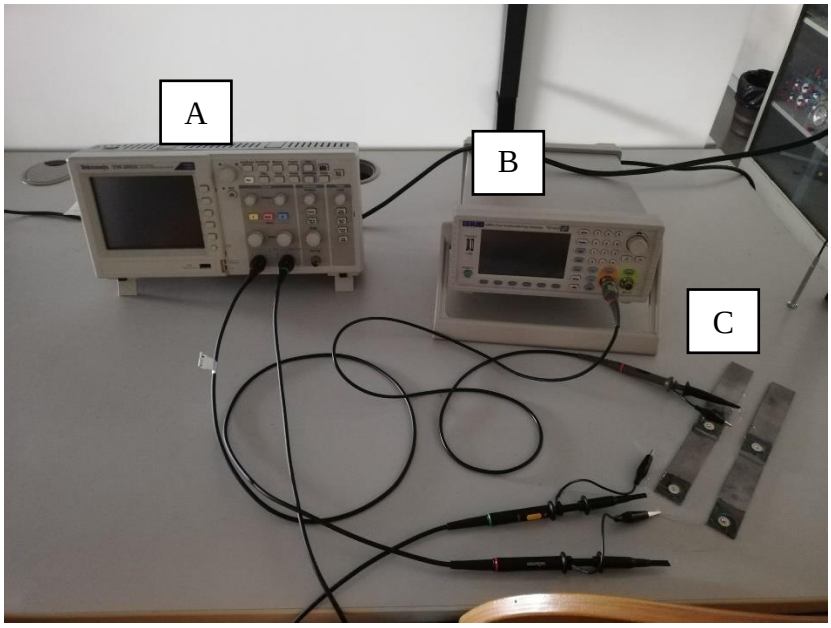


Figure 3.1: Experimental set-up composed by: A – oscilloscope; B - function generator; C - SLJ.

The function generator is responsible for generating the input signal and sending it to the actuator, from the excitation of the actuator LW will be generated and propagated thought the SLJ. The sensor will them capture these waves, and the received signal can be seen in the display of the oscilloscope. The data of the received signal will them be exported from the oscilloscope and imported onto the computer for the post-processing of the data.

The experiments were performed in the laboratory of Electricity at FEUP, Department of Mechanical Engineering, since there is almost an absence of noise and vibration. The piezoelectric sensors are susceptible and can capture these anomalies if they exist.

Five joints were tested, as denoted in Table 3.1.

Table 3.1: Designated name given to every specimen tested.

| Joint name | Defect |
|---|---|
| Joint standard | No defect |
| Joint 2 | No defect |
| Joint 3 | 2 mm void |
| Joint 4 | 4 mm void |
| Joint 5 | 5 mm void |
| Joint 6 | Bad adhesion |

The actuation signal was generated in MATLAB, saved in a CVS file and then imported to the function generator. The PZT captures the signals and using a digital oscilloscope they can be viewed and compared between each other in the time domain.

### 3.1.1 Single lap joint

The manufacturing of the SLJ used a shot blasting machine to clean the substrates (the substrates used are 110 x 25 x2 mm) and generate a good surface for proper adhesion of the adhesive (Figures 3.2 and 3.3). Subsequent, the adhesive was prepared by mixing in the centrifuge the adhesive Av138 with the hardener HV998 in the right proportion, more specifically 100 to 40, for approximately 3 minutes.

Figure 3.2: Shot blasting machine used.

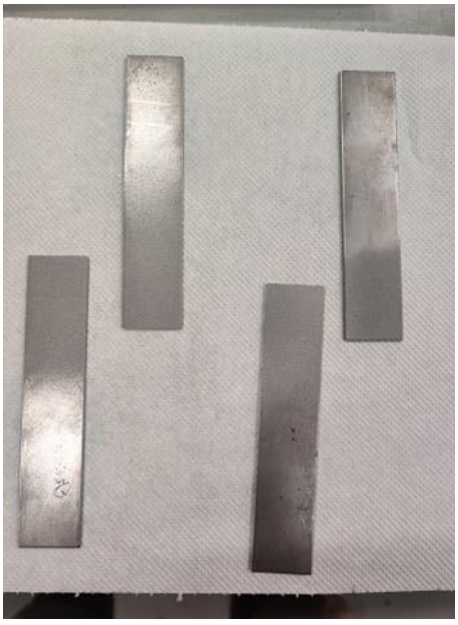

Figure 3.3: Substrates after shot blasting process.

After cleaning the substrates with acetone to remove any impurities, that could affect the adhesion, and having a homogeneous mixture of the adhesive, the substrates were placed in the mold (Figure 3.4), the adhesive was spread on both substrates and joined together with an overlap of 25 mm. Finally, the mold was put in a press and remained there for 24 hours at ambient temperature in order for the adhesive to cure.

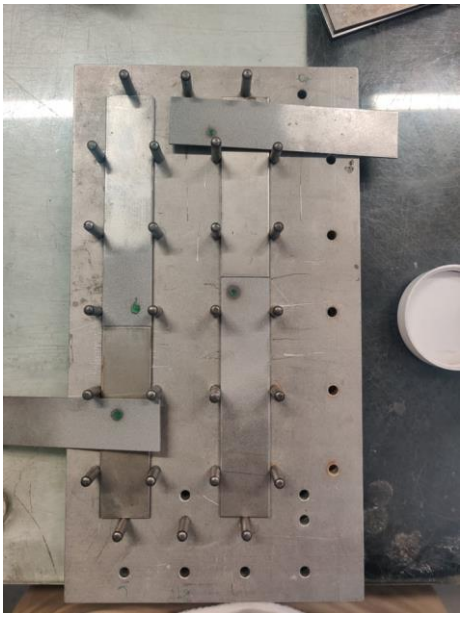

Figure 3.4: Substrates during process of void creation place on top of the mould.

### 3.1.2 Creation of the defects

For the creation of the voids, Teflon fibre circles were cut with a puncture machine (Figure 3.5) with the desired diameter and with a thickness of 1 mm. Then, the circle-shaped Teflon fibre was glued on the substrates, in the coordinates (93.25, 8.75) mm before the application of the adhesive. Due to this process having been executed manually, the void location does not possess high accuracy.

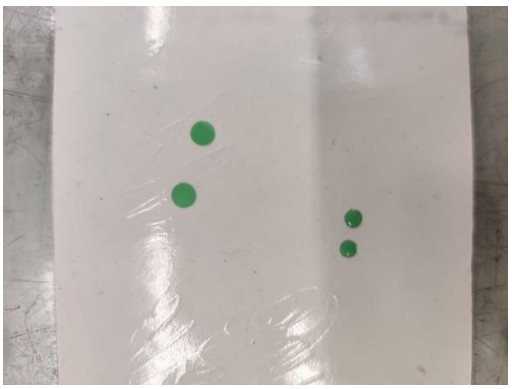

Figure 3.5: Teflon fibre circles used to generate the void in the SLJ.

For the creation of the weak adhesion in SLJ, both substrates were dipped in a release agent before the application of the adhesive. The release agent acted as a contaminant and jeopardized the adhesion between the SLJ and the substrates.

### 3.1.3 Function generator

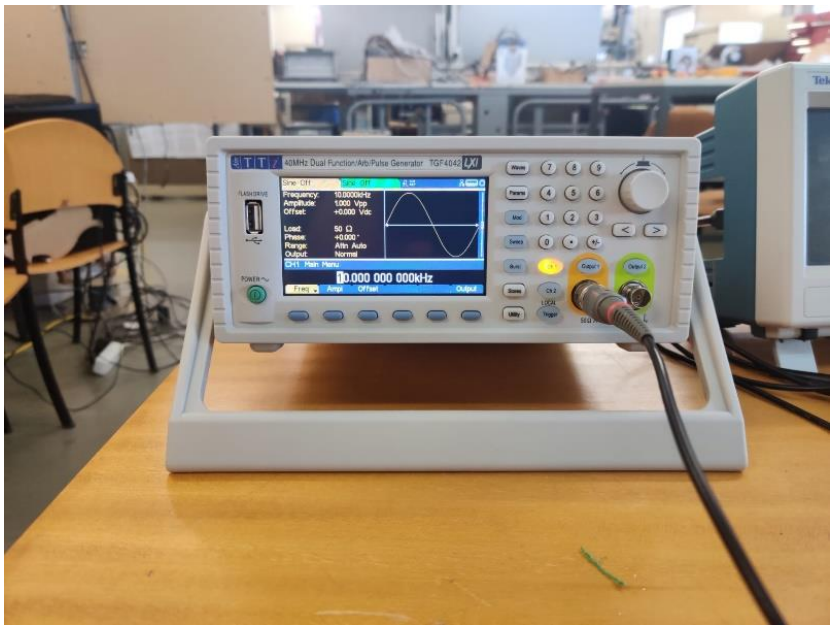

Figure 3.6: Function generator TGF4042.

The function generator TGF4000 series (Figure 3.6) was used in this experimental procedure. This device offers a signal generation capability of up to 240 MHz on two identical full performance channels, with a phase control resolution of 0.001° from channel to channel.

It includes a wide range of built-in waveforms and can import arbitrary waveforms generated by specific PC based software. For the experiments, the excitation signal was primarily created in MATLAB and, afterwards, imported to the function generator. An internal trigger source applies the signal previously generated to the piezoelectric actuator [38].

The trigger was set to manual, and the amplitude of the input signal was increase ten times so that the signal received by the sensor could be more easily detected.

### 3.1.4 Osciloscope


Figure 3.7: Oscilloscope Tektronix TDS 2002C.

The oscilloscope used in the experiments is the Tektronix TDS 2002C (Figure 3.7). This device possesses various features that help to achieve good performance, such as:

- A digital real-time sampling that accurately captures signals with at least ten times oversampling on all channels.
- A waveform limit testing that eliminates mistakes with the pass/fails summary table;
- A USB PC connectivity that allows to easily connect to a personal computer with the rear-panel USB device port. Using NI LabVIEW SignalExpress™ software, one can control the scope, log data, transfer and document the results.
- It has two analogue channels, with a record length of 2.5 K points, a sample rate of 2 GS/s, allowing it to plot in the same display the input signal and the sensor's signal.

Despite the feature of the NI Lab VIEW SignalExpress, a different software to export the log data and the scope to the PC was used, the *OpenChoice desktop* from Tektronix. This software allows one to save the results in a CSV format for the data post-processing. This file can then be imported to MATLAB, where the data can be analysed, plotted and compared with the signals from different SLJ, with and without defect.

### 3.1.5 Piezoelectric sensors

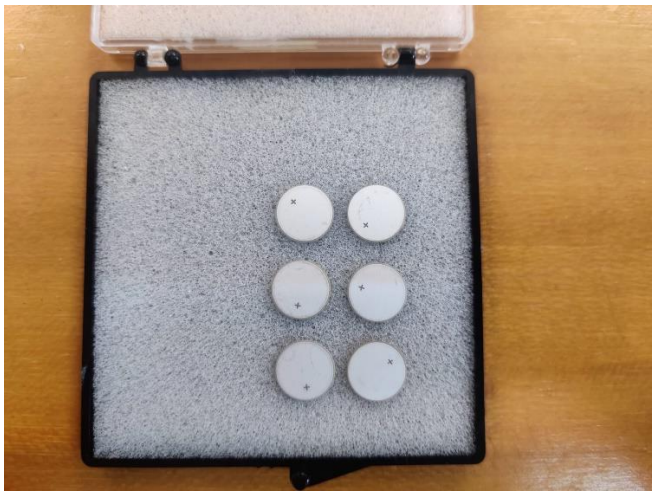

Figure 3.8: Piezoelectric sensors Type pz24.

The piezoelectric sensors used were disc type pz24, manufactured by Meggitt (Figure 3.8). This type of sensor has a positive and negative side in the upper and lower surfaces of the disc, respectively.

Therefore, in order to glue the sensor to the SLJ, the first approach was using an electric conductive glue such as liquid silver. However, no conductive glue was easily attainable. Therefore, an attempt was made to glue the sensor by mixing super glue with small particles of iron in order to transform the glue into a conductive material. This attempt ended up not working, since the small particles of iron started reacting with the glue and agglomerated, forming a layer of solid particles blocking the adhesion to the bottom surface of the sensor.

In a second attempt, it was used a copper wire and a thicker glue (adhesive MA 442 plexus) to resolve the problem. The copper wire would grant the conductivity and the connection with the lower surface of the disc. The ticker glue resolved the problem of the adhesion. The thickness was an essential factor since the copper wire is embedded in the adhesive, as shown in Figure 3.9.

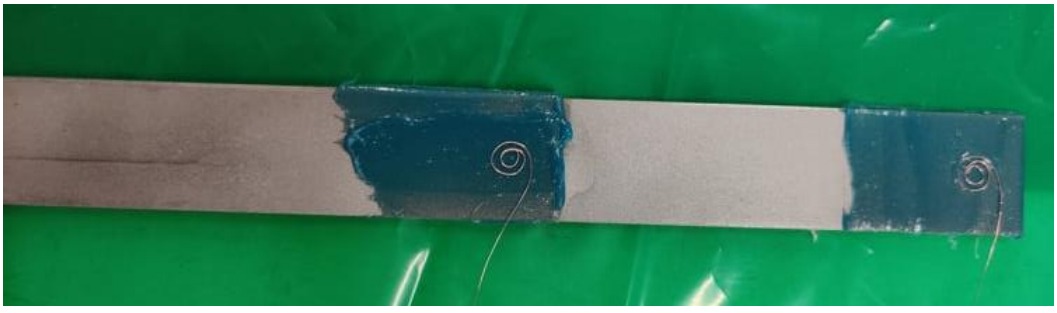

Figure 3.9: Copper wire used between the substrate and the sensor glued with the adhesive MA 442 plexus.

After embedding the copper wire in the adhesive, the sensor was placed on top of it. Then the pressure was applied for 24 hours with the spring until the adhesive was fully cured. Afterwards, another copper wire was welded to the upper surface of the piezoelectric sensor, to establish the connection with the positive side of the sensor, as shown in Figure 3.10.

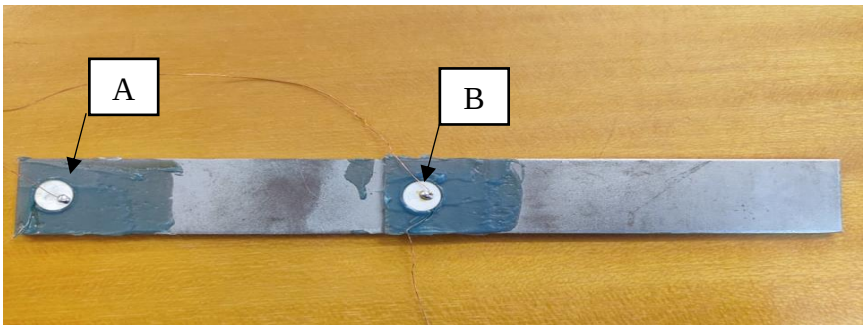


Figure 3.10: A - Sensor ; B - Actuator.

The PZT sensors were used to generate and received the LW. In each test, one sensor was used as an actuator and the other as a sensor. The actuator was always located on top of the overlap part and the sensor at the edge of the SLJ (Figure 3.10). The sensors were connected by wires to the function generator or the oscilloscope, depending on their role in the test.

### 3.1.6 Actuation signal

Taking into consideration the dispersive nature of LW, the actuation signal needs to excite only one mode. If more than one wave mode is excited, LW with various velocities are obtained, and the obtained results will become too complicated for interpretation. In order to choose the appropriate signal for LW excitation, several signals were considered. Thus, the best result corresponds to a Hanning window multiplied by a sinusoidal signal, as shown in Figure 3.11.

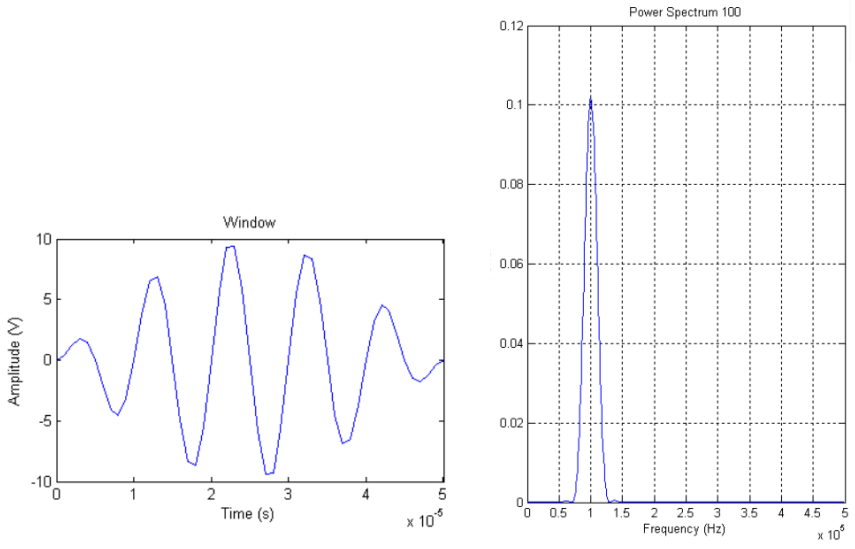


Figure 3.11: Hanning window multiplied by a sinusoidal signal and respective power spectrum.

The Hanning window is given by,

$$F = A * \sin(2\pi f t) * sin\left(2\pi \frac{f}{10} t\right) \quad (3.1)$$

where, $A$ is the amplitude, $f$ is the frequency, and $t$ is the time instant.

The Hanning window tone burst's power spectrum shows a broader main frequency peak, and there is almost no sideband. In this case, the frequency component is concentrated around the main peak, reducing the frequency spread range.

In Figure 3.11, the wave shown is the theoretical wave generated in MATLAB. Therefore, the wave sensed by the sensor can be seen in the oscilloscope and is represented in Figure 3.12.

This wave has generated with a frequency of 40 kHz and with an amplitude of 10 V.

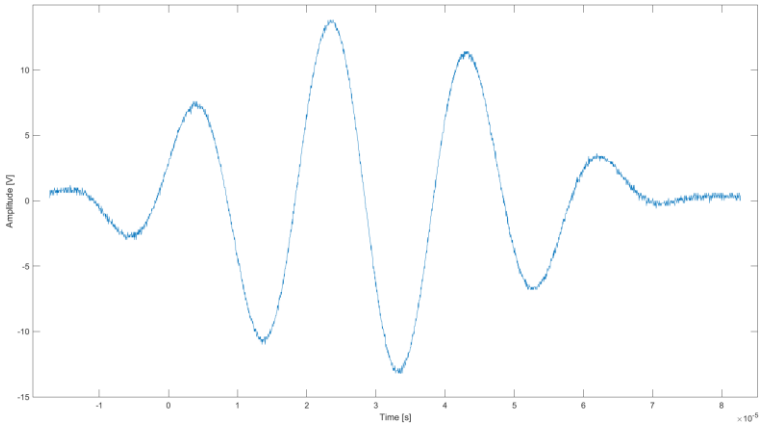


Figure 3.12: Signal generated by the function generator provided to the actuator.

### 3.1.7 Experimental results

As previously referred, six adhesively bonded joints were tested and, to better understand the influence of damage, each one was compared with the standard joint, which is a normal SLJ without any defect. Each test was performed five times in order to guarantee repeatability and to choose the signal with the least influence of noise for the comparison.

For the first round of tests, the standard joint was compared with another SLJ without defect (Joint 2) in order to discover if there was repeatability (Figure 3.13).

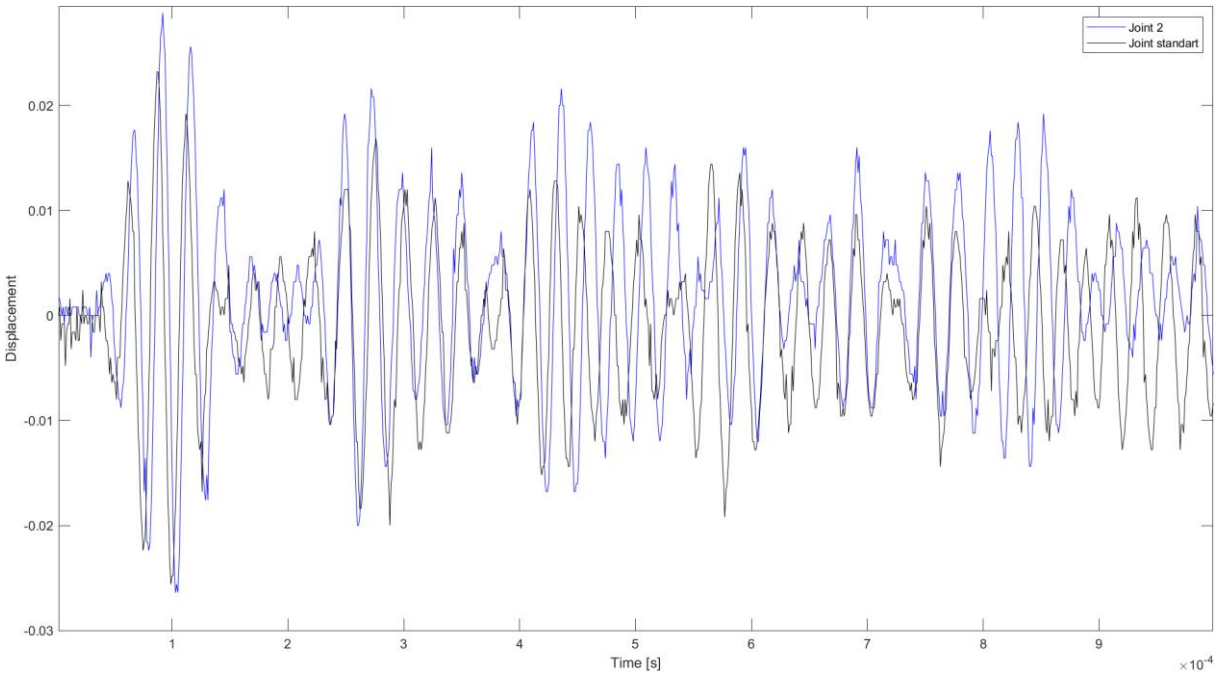


Figure 3.13: Plot of standard Joint (Blue) versus Joint 2 (Black).

As one can see, the signals have some discrepancies, although this phenomenon can be attributed to the fact that bonding of the PZT sensor is manually done. As such, the force applied to bond the sensor is uncontrolled, making the PZT element somewhat prone to cracking, which occurred here. Furthermore, the application of the adhesive layer between the substrate of the SLJ and the sensor is also done manually, and, consequently, limited control on the adhesive thickness can be achieved, at best. Higher thicknesses make the PZT sensors less sensible to the measurement of LW, and the PZT actuator loses the capability of exciting these waves.

One can conclude from these experiments that mechanical repeatability can be achieved, since LW modes can still be excited and measured. However, this repeatability is also a function of the sensor's integrity, of their exact location in the SLJ, and of the adhesive's layer thickness that allows the connection of the sensor to the structure.

After this verification, the rest of the joints were tested. Figures 3.14, 3.15 and 3.16 represent the signals comparing the standard joint with Joint 3, 4 and 5, respectively.

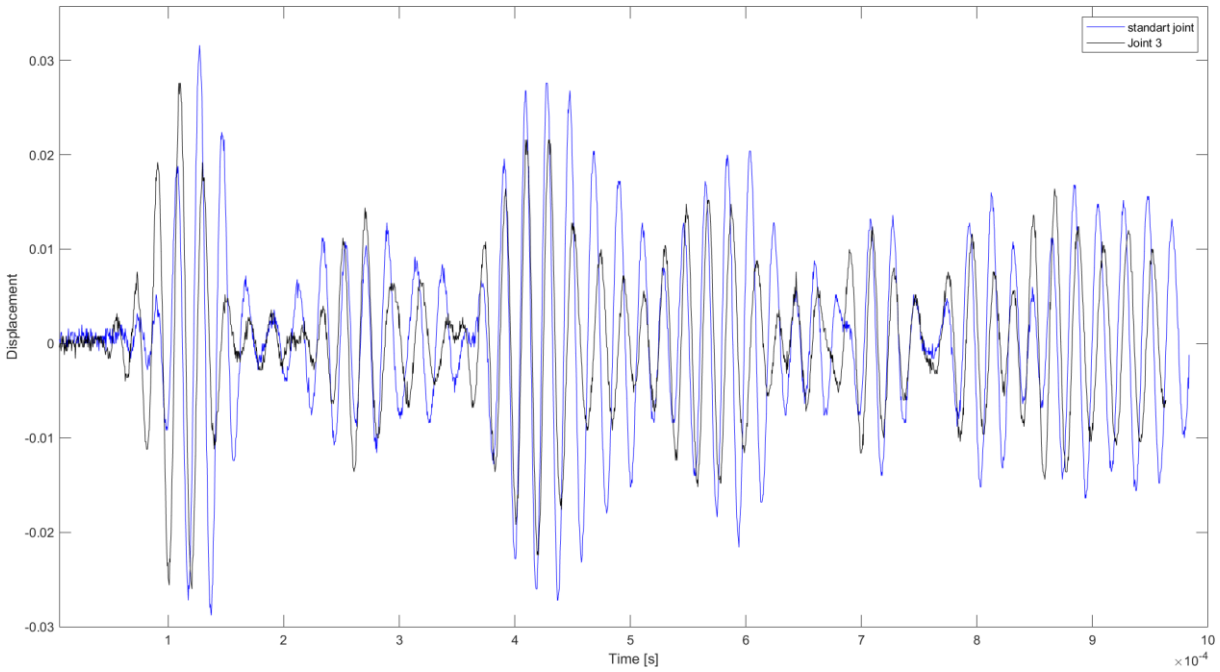


Figure 3.14: Plot of standard Joint (Blue) versus Joint 3 (Black).

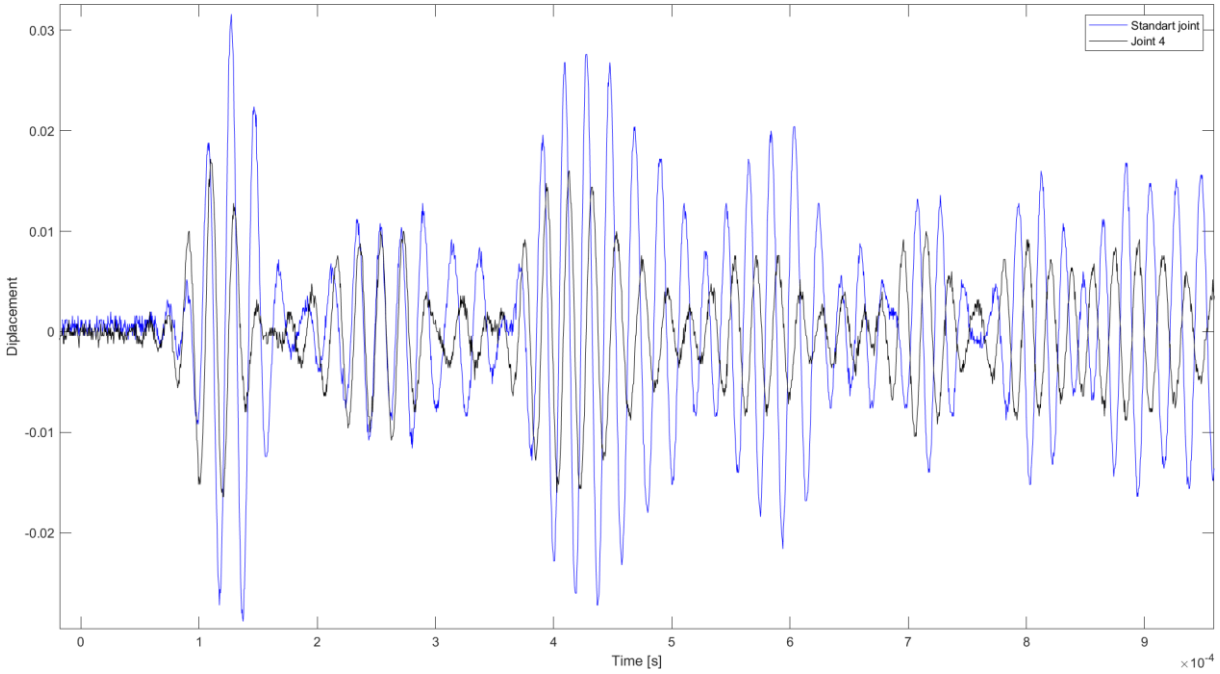


Figure 3.15: Plot of standard joint (Blue) versus Joint 4 (Black).

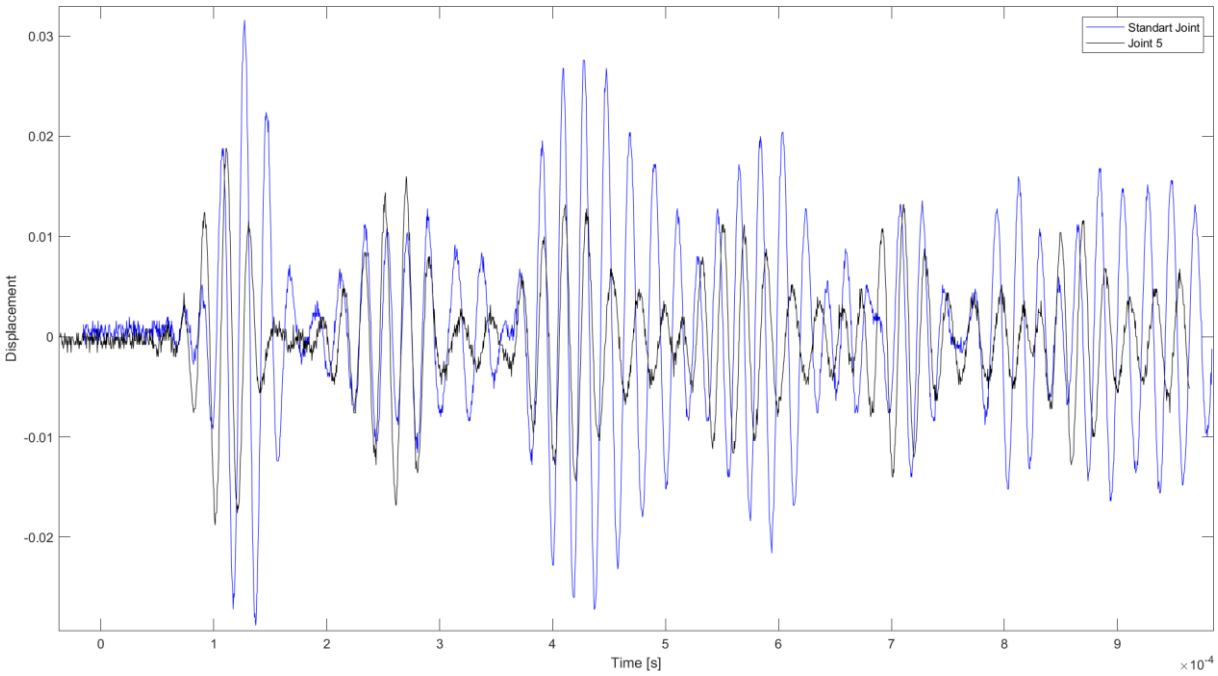


Figure 3.16: Plot of standard Joint (Blue) versus Joint 5 (Black).

Analysing Figures 3.14, 3.15 and 3.16 one can conclude that the detection of damage is visible once there is a change in magnitude of the wave. This difference in displacement can indicate the presence of a void and, as it will be observed in chapter 4.3, there is a relation between the size of the damage and the difference in amplitude between the obtained signals.

In order to understand the capabilities of this method, LW were also used in a SLJ with weak adhesion. This joint was created by dipping the substrate in release agent before applying the adhesive. The results are shown in Figure 3.17.

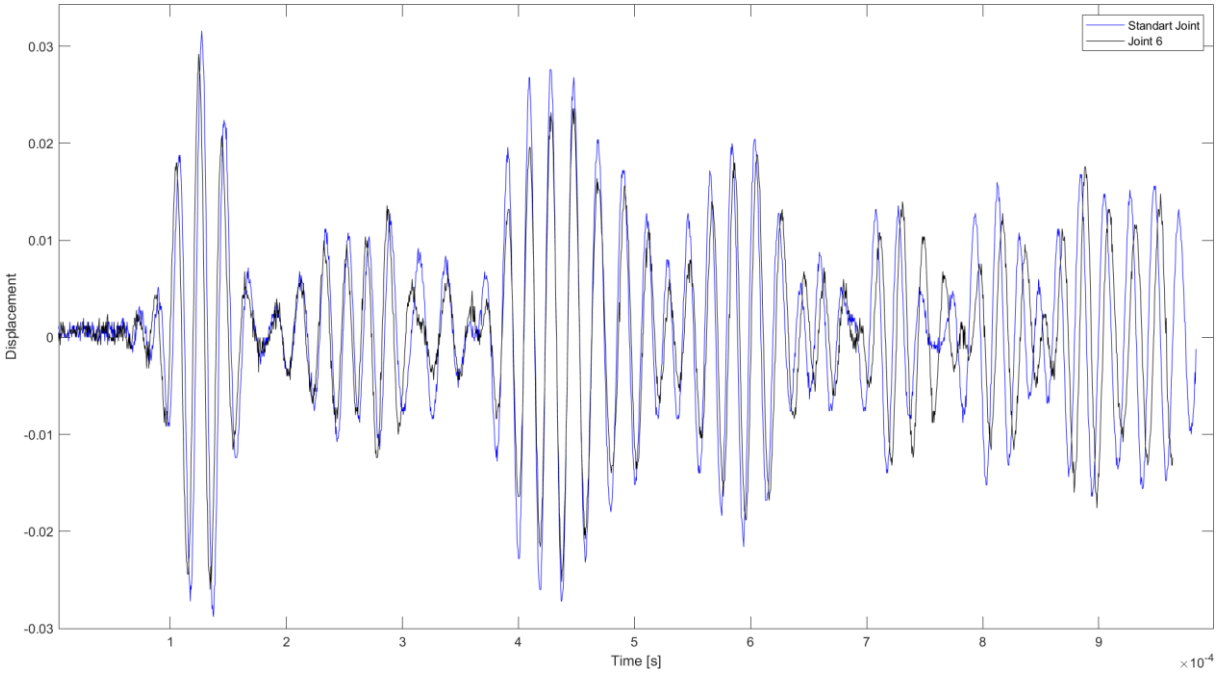


Figure 3.17: Plot of standard joint (Blue) versus Joint 6 (Black).

As seen in Figure 3.17 the results shown a minor difference between the signals, more specifically during 4 to $5x10^{-4}$ s. This difference is not sufficient to conclude that this method of analyses detects this kind of defect. However, it may be possible to detect this type of defect using other methods base on a frequency domain analysis.

### 3.1.8 Destructive tests

After finishing all the experimental tests, a destructive test was performed on all specimens to verify the results' veracity.

Therefore, the specimens were placed into an oven at a temperature near the 300ºC to weaken the adhesion properties. After approximately 15 minutes, the specimens were taken out and applied a torsional force manually to separate the adherends. Figure 3.18 shows an example of one of these tests and clear signs of a defect in the adhesive layer.

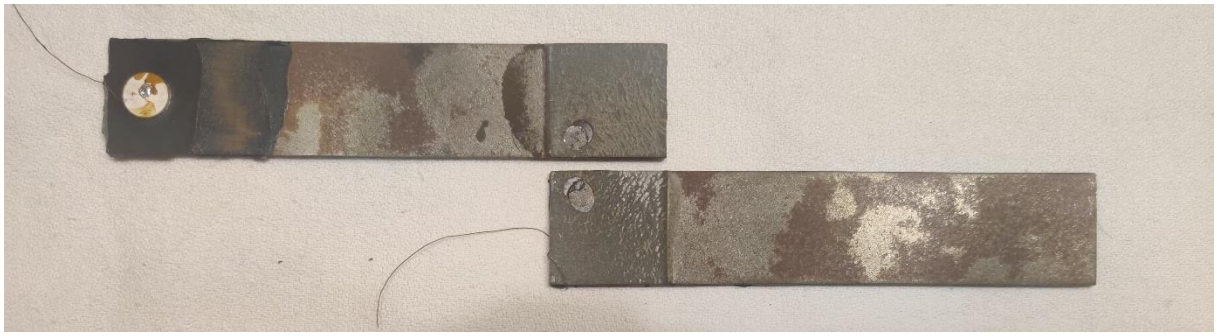

Figure 3.18: Joint 5 after the destructive test.

At the end of this procedure, it was concluded that all the voids were accurately placed at the desired coordinates, proving that the manufacturing process was well executed.

For the Joint 6 is was performed a tensile test, and the results confirmed the weak adhesion. As seen in figure 3.19, for the weak adhesion joint, the withstand load is approximately 900 N as for a standard SLJ that value is much higher, more specifically 7000 N.

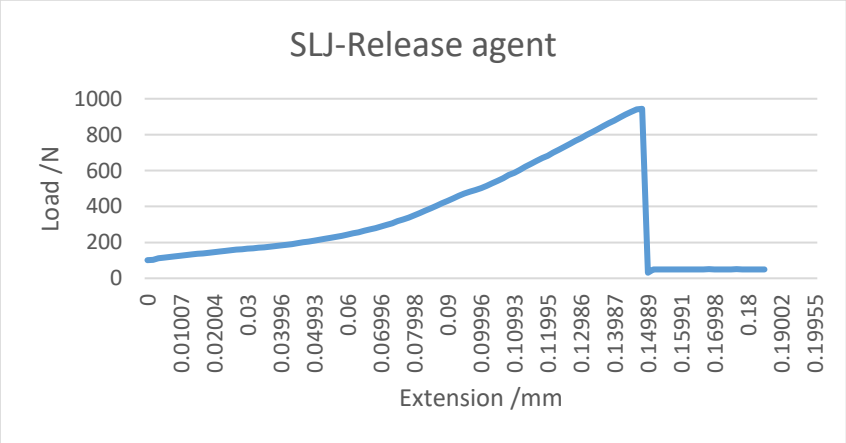


Figure 3.19: Joint 6 tensile test results.

# 4 Numerical simulation

In order to validate the experimental results and understand the effect of LW in SLJ, two different sets of numerical models were created. Numerical simulations of the wave propagation process were performed using the program ABAQUS CAE.

The first simulated set was a 2 mm aluminium plate with a dimension of 500 x 500 mm. This simulation was created due to its simplicity and to define the methodology to create the SLJs.

The other part of the simulation work girds up to the single lap joint and the detection of the void embedded in the adhesive.

Several parameters were changed, such as frequency, sensor location, void location, mesh size, step time, and load orientation, to determine the optimal values, in order to achieve accurate results.

## 4.1 Simulation of the aluminium plate

The first model tested was a 500 x 500 mm aluminium with a 2 mm thickness (Figure 4.1). This model was chosen due to its oversized dimensions providing a well-described signal with a minimal overlay of LW modes, and due to being a homogeneous model, increasing the ease to analyse the data collected, as reported in [29]. This model gave the freedom to test many possible combinations of parameters and helped to reach the optimal result. It was also used to make some conclusions regarding the effect of the damage location and size, in the propagation LW.

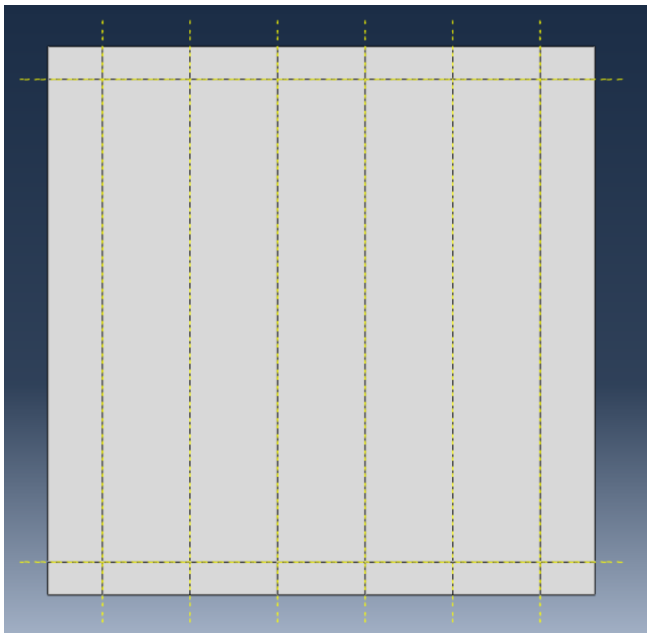

Figure 4.1: Aluminium plate model.

### 4.1.1 Sensor location

Twelve sensors were placed through the plate to represent and work as piezoelectric sensors to study this model. The location of the sensors is discriminated in Table 4.1.

Table 4.1: Localization of the sensors placed in the Aluminium plate model.

| sensor | X coordinate (mm) | Y coordinate (mm) |
|---|---|---|
| **1** | 450 | 470 |
| **2** | 370 | 470 |
| **3** | 290 | 470 |
| **4** | 210 | 470 |
| **5** | 130 | 470 |
| **6** | 50 | 470 |
| **7** | 450 | 30 |
| **8** | 370 | 30 |
| **9** | 290 | 30 |
| **10** | 210 | 30 |
| **11** | 130 | 30 |
| **12** | 50 | 30 |

### 4.1.2 Properties

The velocity of LW depends on the properties of the material, as seen in equations (2.4) and (2.5). The definition of the material is fundamental since LW travel differently depending on the material. As such, in this simulation, three material properties need to be specified: the density, the young's module, and the Poisson's ratio.

The material used in the simulation of the plate was aluminium, and their properties are represented in Table 4.2.

Table 4.2: Aluminium Properties.

| | **Aluminium** |
|---|---|
| **Density** | 2.5 g/ $cm^3$ |
| **Young's module** | 62 GPa |
| **Poisson´s Ratio** | 0.33 |

### 4.1.3 Frequency

The frequency of the input signal is a crucial parameter to define and should be high enough to avoid possible overlap of waves at the piezoelectric sensor. As previously seen in Chapter 2, the group velocity of LW is dependent on the wave's frequency. Therefore, if a wrongful definition of the wave's frequency is made, then there can be an overlap of various waves (reflected waves and directly transmitted wave from the actuator to the sensor). This can difficult the detection of damage since the superposition of various waves can hide the perturbations caused by the presence of damage.

On the other hand, the chosen frequency cannot be too high since a higher frequency implies a smaller wavelength, thus affecting the resolution of the numerical model.

As such, input signals with frequencies between 20 kHz and 200 kHz were used, being the 40 kHz input signal the excitation signal that presents the most promising results. Contrary to the other frequencies, at 40 kHz, the response signal obtained did not present any significant perturbations or more than one frequency excited, as shown in Figures 4.2 and 4.3. Due to this fact, all further research was done with an input signal with a frequency of 40 kHz.

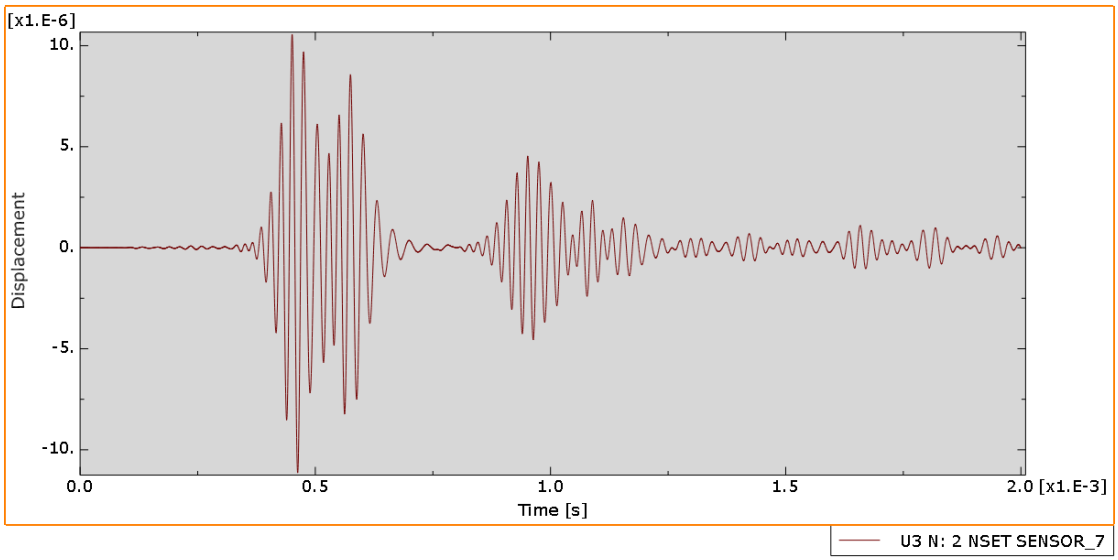


Figure 4.2: Measured signal at sensor 7, where wave was generated at sensor 1 with frequency of 40 KHz.

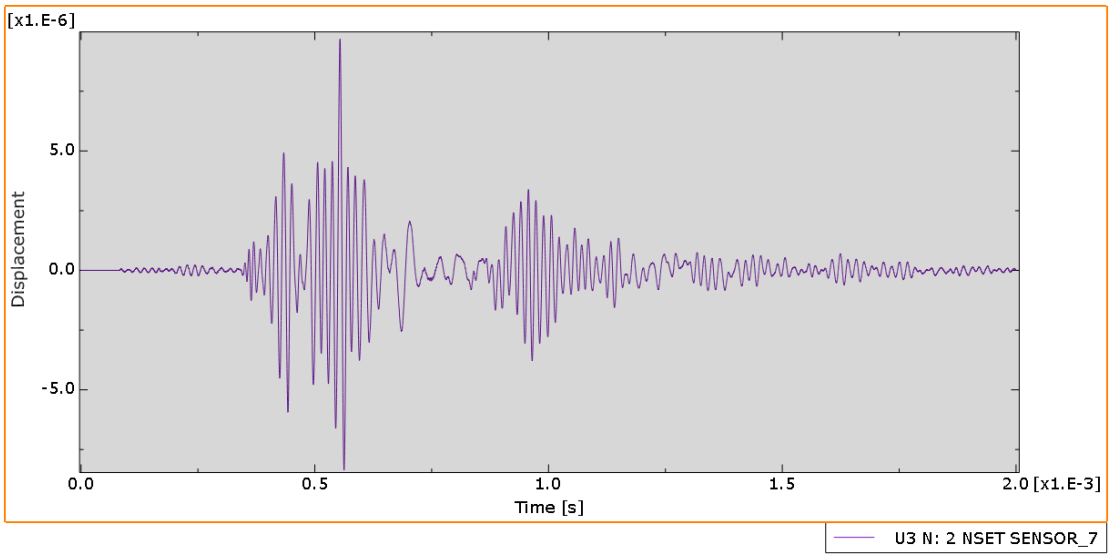


Figure 4.3: Response of sensor 7 with the actuator on sensor 1 at a frequency of 60 kHz for the aluminium plate.

### 4.1.4 Step and step time

The time of simulation is crucial because of complex wave propagation and reflection dynamics. The time of simulation needs to be big enough so that the sensors can receive the reflected waves.

The correct choice of step time is crucial to obtain accurate results. The more complex the model is, the smallest the step time needs to be. For all models, a variable step time was used, implying that for further analysis of the numerical results, it is needed to interpolate the results to obtain data for equal time intervals.

Using a time of simulation of 0.003 s and preforming an Explicit Dynamic simulation, it was possible to reach to results shown in section 4.2.

### 4.1.5 Mesh size

The wavelength determines the mesh size and, as such, by the excitation's frequency used. The wavelength varies with the material due to the wave's propagation speed, also called phase velocity.

To obtain the value of wavelength, a MATLAB based software called *Dispersion calculator* was used. After specifying the material and thickness, this program plots the graph of the wavelength as a function of the frequency, thus obtaining the value of the wavelength for 40 kHz directly for the aluminium plate. Figure 4.4 presents the graph that relates the wavelength with the frequency for the aluminium plate.

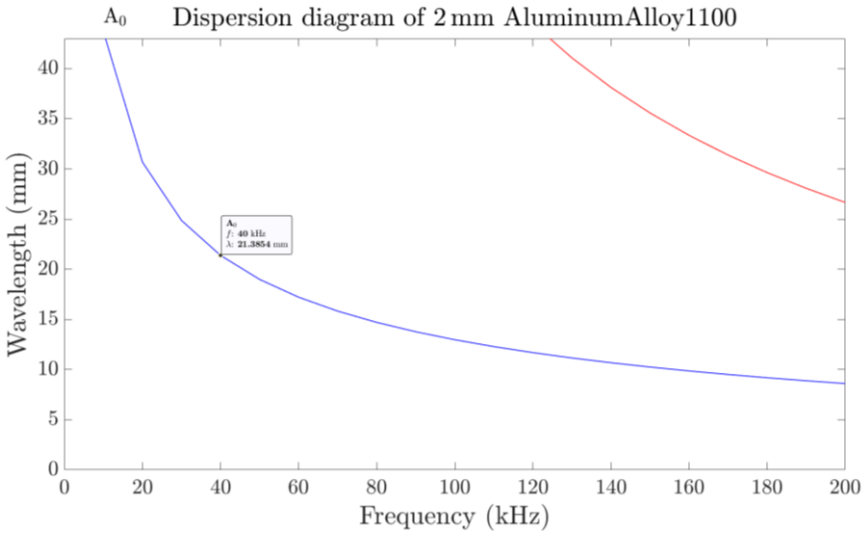


Figure 4.4: Graph of the dispersion curve of an aluminium plate with 2 mm thickness.

For a suitable resolution and trustworthy simulation, the mesh size needs to be approximately ten times smaller than the wavelength. Therefore, for a 40 kHz frequency in a 2 mm aluminium plate, the wavelength and the mesh size are shown in Table 4.3.

Table 4.3: Wavelength and advisable mesh size for a 40 KHz frequency in a Aluminium plate with 2 mm thickness.

| | **Aluminium** |
|---|---|
| **Wavelength** | 21.38 mm |
| **Mesh size** | 2.138 mm |

These gives a recommended mesh size of 2 mm, which results in a mesh of 250 x 250 nodes (62500 nodes).

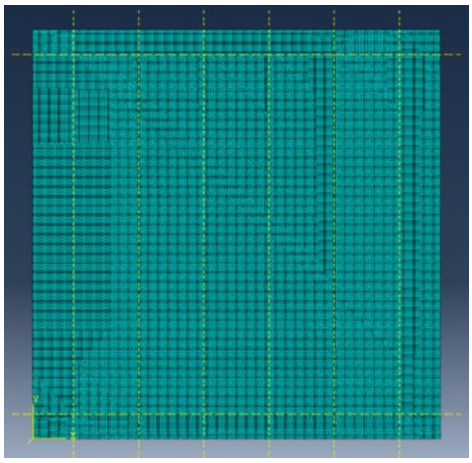

Figure 4.5: Representation of the mesh size used in the aluminium plate model.

### 4.1.6 Results - Aluminium plate

The first set of tests with this numerical model girds up to the location of the damaged despite the location of the defect. The simulated defect for this round of tests was a hole with a diameter of 5 mm and was placed in one of three different locations shown in Table 4.4.

Table 4.4: Coordinates of the defects generated for the aluminium plate.

| | X coordinate (mm) | Y coordinate (mm) |
|---|---|---|
| **Defect 1** | 50 | 415 |
| **Defect 2** | 65 | 415 |
| **Defect 3** | 335 | 260 |

The chosen actuator for this test was sensor 1 (as defined in table 4.1) and the results of this experiment are shown in Figures 4.6, 4.7 and 4.8.

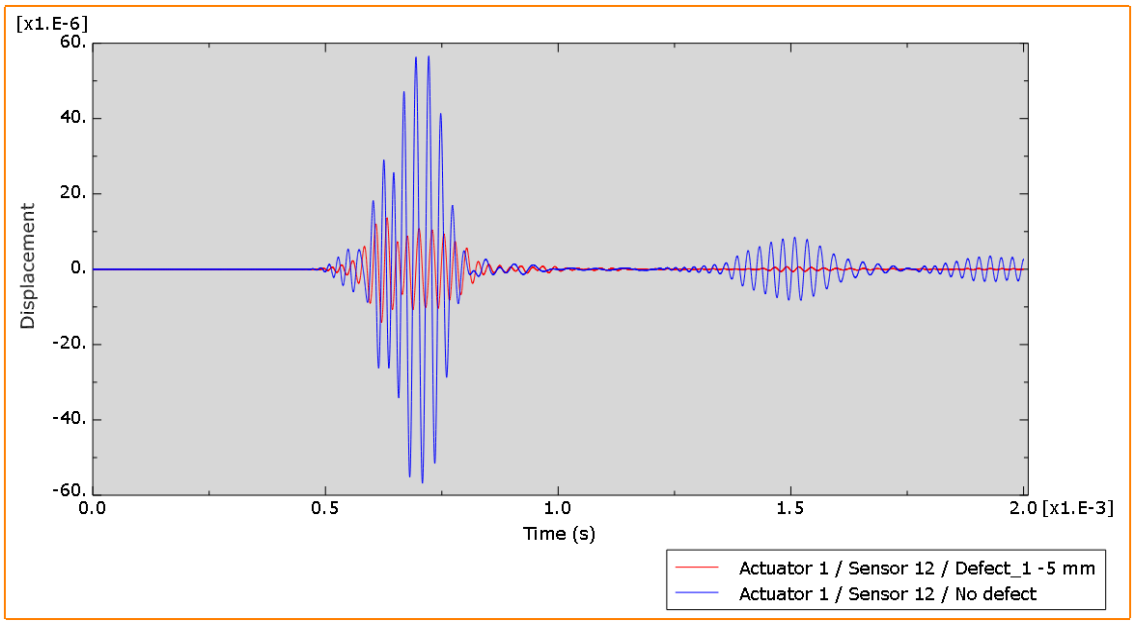


Figure 4.6: Plot of the measured signals by sensor 12 with Defect 1and without defect.

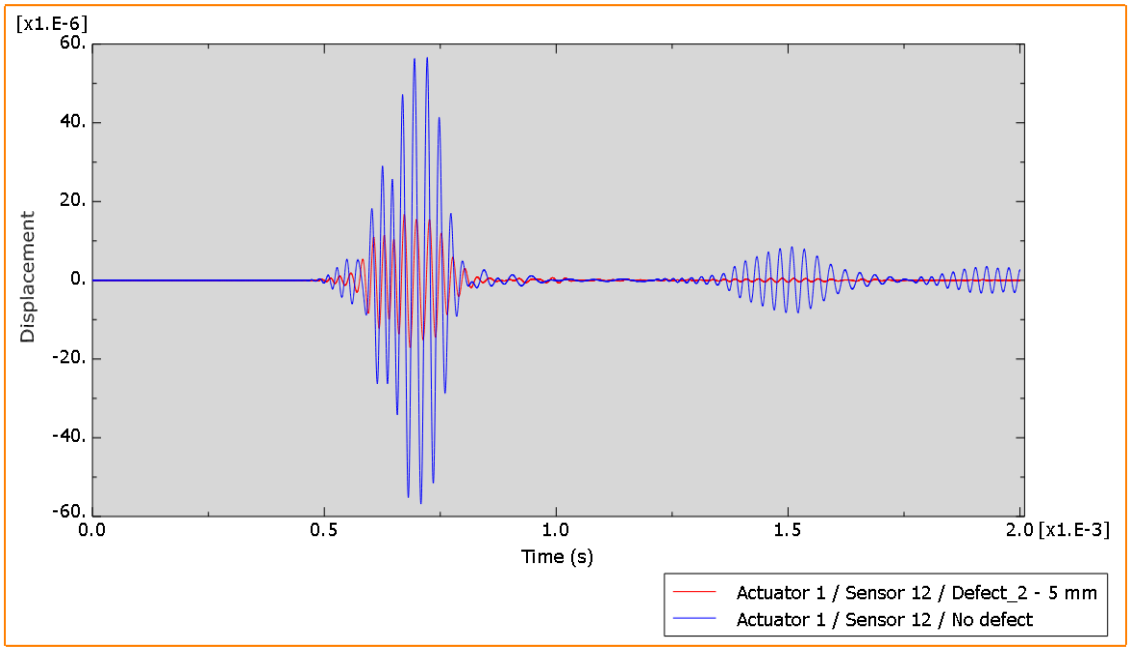


Figure 4.7: Plot of the measured signals by sensor 12 with Defect 2 and without defect.

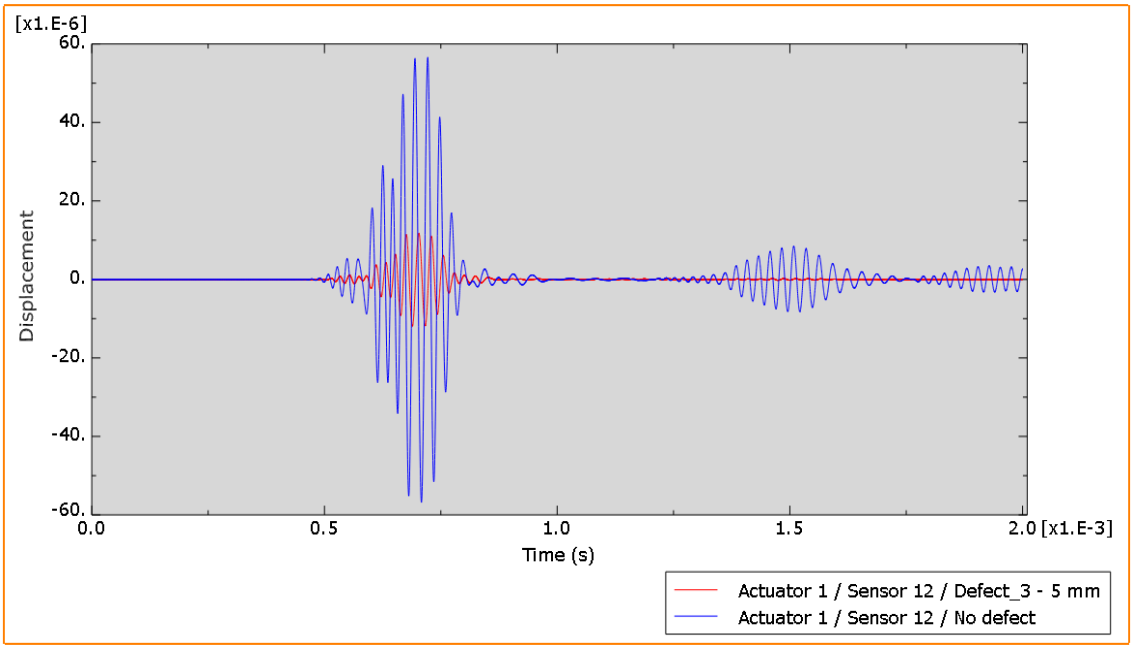


Figure 4.8: Plot of the measured signals by sensor 12 with defect 3 and without defect.

By analysing these figures, one can conclude that, despite the void's location, the LW can detect the damage. Thus, one can see a clear difference in particle displacement due to the influence of damage.

Having established that the detection of damage is possible for any given damage location, the next simulations will determine what damage location has a more significant impact in analysing the data. In theory, if one considers the wave's direct path, the difference between displacement's amplitude in the damaged and normal specimen's augments as the distance between the focus of damage and the direct path decreases. Therefore, a test was

performed comparing the data collected by the sensors when a defect is present in the direct path of the wave or not.

For this test, it was used the Defect 1's location (as per Table 4.1) and preform a simulation using the piezos 1 and 6 as actuators and piezos 7 and 12 as the respecting sensors.

Figure 4.9 presents the obtained results regarding this test, where only one of the input signals for the simulation without defect is represented thus being symmetrical and consequently identical.

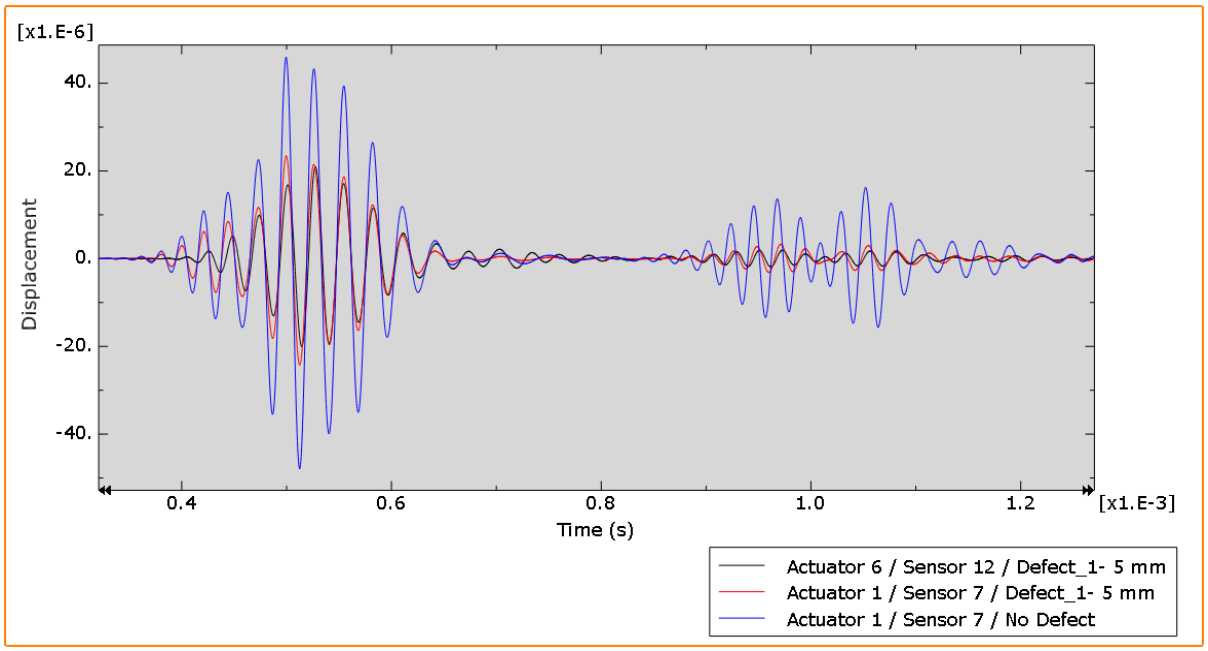


Figure 4.9: Plot of the signals measured by sensors 7 and 12, without damage and with Defect 1 (actuators are, respectively, sensors 1 and 6).

Once proven that the localization of the defect influences the measured wave, the next step is to analyze the influence of the increase in damage size. Therefore, and using the location of Defect 1, as indicated in Table 4.1, the void size will be increased. Firstly, three different sizes were tested (5 mm, 10 mm, and 15 mm) using sensors 6 and 12 as actuator and transducer respectively, since this combination is the most sensible to the presence of damage.

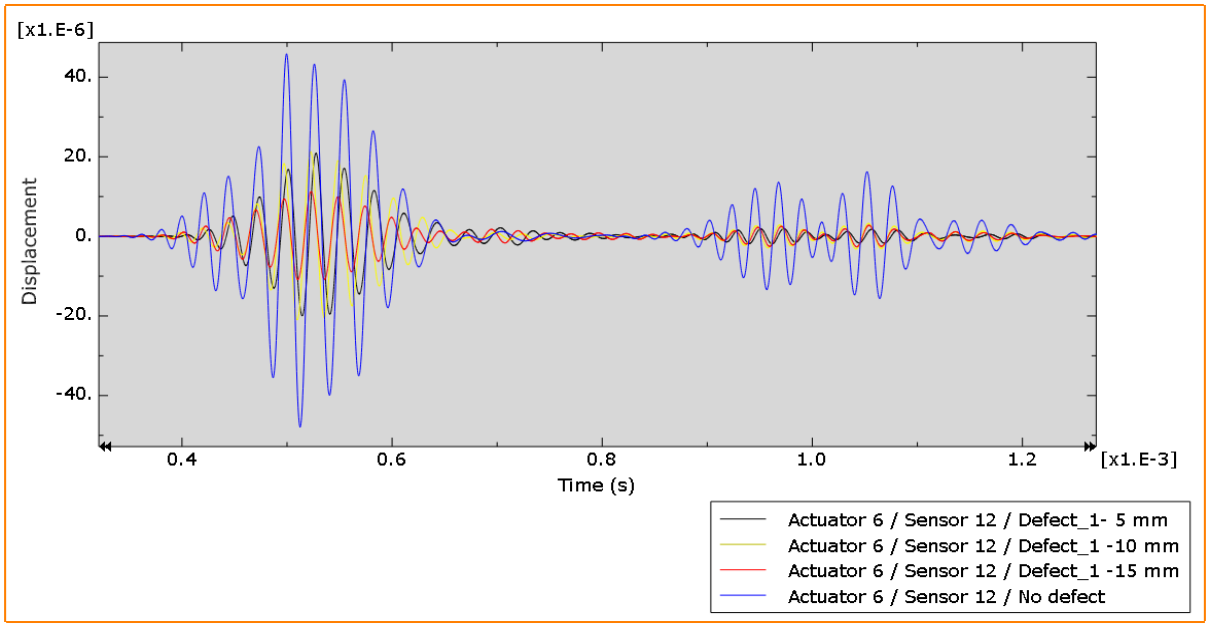


Figure 4.10: Plot of the signals measured by sensor 12, where sensor 6 behaved as LW actuator, without damage and with damage in location Defect 1, and various sizes.

In order to achieve this, the number of simulations had to increase to obtain more data and, as such, to see if one can see a trend with these indices. Consequently, various simulations were performed with a void size from 5 to 45 mm. The calculated indices were the signal Sum of Squared Differences, SSSD given by

$$DI = \frac{\sum(S_H - S_D)^2}{\sum {S_H}^2} \tag{4.1}$$

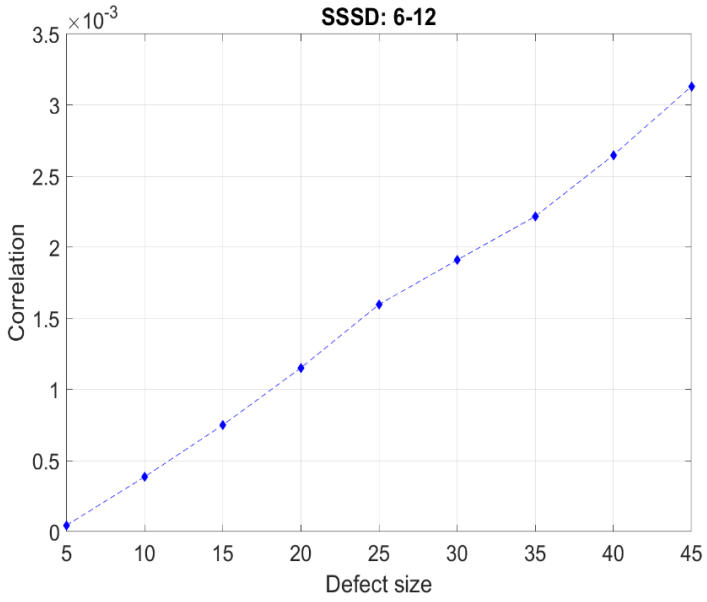


Figure 4.11: Plot of the SSSD index, where Sensor 6 is the actuator and Sensor 12 is the Transducer.

and the Correlation Coefficient, CC, given by

$$\rho = \frac{\sum_{i=1}^{n}(X_i - \bar{X})(Y_i - \bar{Y})}{\sqrt{\sum_{i=1}^{n}(X_i - \bar{X})^2 \cdot \sum_{i=1}^{n}(Y_i - \bar{Y})^2}} \tag{4.2}$$

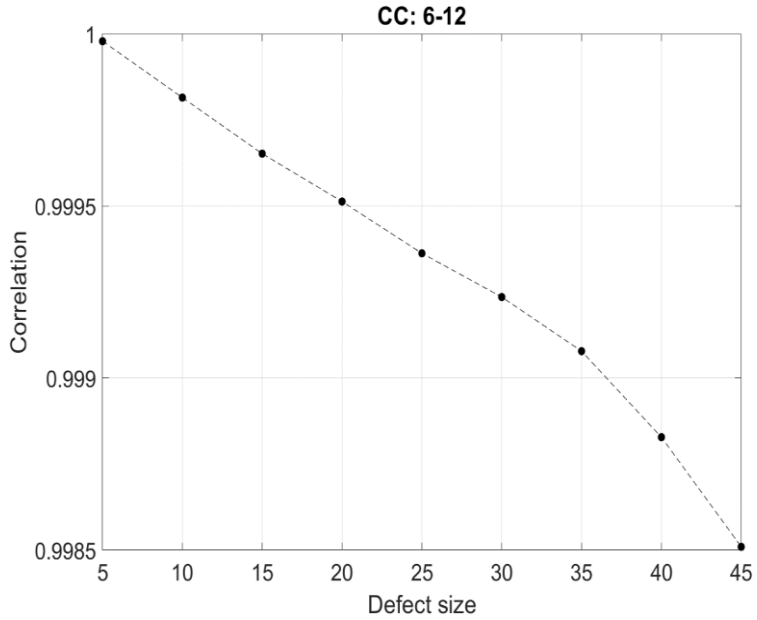


Figure 4.12: Plot of the CC index, where Sensor 6 is the actuator and Sensor 12 is the Transducer.

As seen in Figures 4.11 and 4.12, the index SSSD has a growing trend with the increased damage, whilst the CC index decreases. These indices, combined with TOF, provide an approximate value of the defect's size and location. Since the TOF determines the approximate location of the damage by comparing the reflexions of the received signals with and without defect.

## 4.2 Simulation of the SLJ

As previously mentioned, a model of a SLJ with an overlap of 25x 25 mm (SLJ_25x25) was created, as shown in Figure 4.13.

The SLJ substrates have a dimension of 120 x 25 mm with a 2 mm thickness. The adhesive layer has a 25 mm overlap and a 0.2 mm thickness.

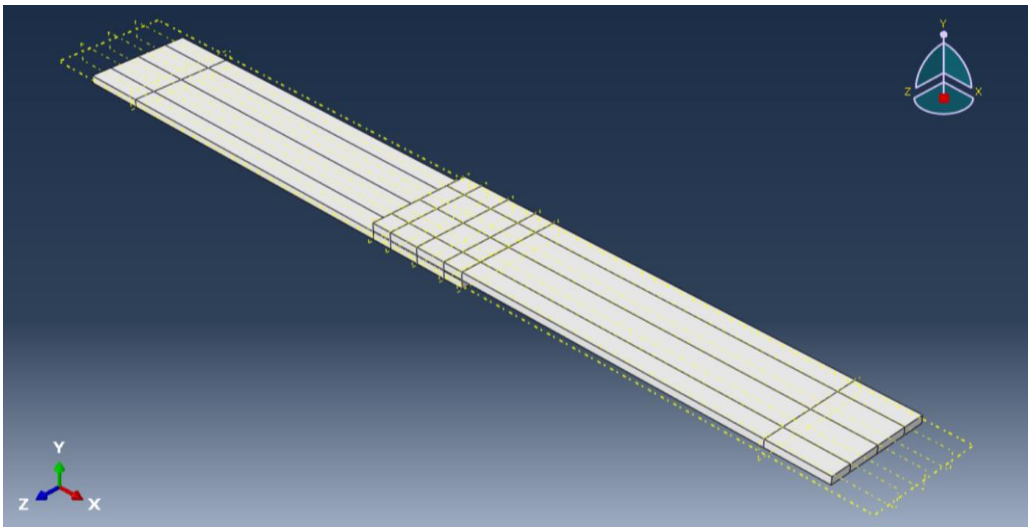


Figure 4.13: Numerical model of the SLJ.

### 4.2.1 Sensor location

Two sensors were placed in the SLJ model, as equivalents to the piezoelectric actuator and transducer. Their location is discriminated in Table 4.4.

Table 4.5: Coordinates of the sensors placed at the SLJ.

| | SLJ_25x25 | | |
|---|---|---|---|
| | **X coordinate (mm)** | **Y coordinate (mm)** | **Z coordinate (mm)** |
| **Sensor_1** | 107.5 | 4.2 | 12.5 |
| **Sensor_2** | 10 | 2 | 12.5 |

Depending on each type of simulation, one of these sensors would function as an actuator as the other as a sensor.

### 4.2.2 Properties

For this numerical model, two different materials were used one for the substrates and the other for the adhesive.

The material used for the substrates was steel and for the adhesive was the AV138 in resemblance to the experimental work.

Table 4.6: Properties of the adhesive and substrates.

| | **Steel** | **Adhesive (AV138)** |
|---|---|---|
| **Density** | 7.8 g/cm$^3$ | 8.7e-1 g/cm$^3$ |
| **Young's module** | 210 GPa | 4.590 GPa |
| **Poisson's Ratio** | 0.33 | 0.35 |

### 4.2.3 Frequency

In chapter 4.1.3 was established the best frequency for this type of simulations (40 kHz). Accordingly, the same criteria were applied to this one. Therefore, all tests with this model were generated with an input signal with a frequency of 40 kHz.

### 4.2.4 Mesh size

The method used to determine the mesh size is the same as for the aluminium plate model. The dispersion curves for the stainless steel and the adhesive are represented in Figures 4.14 and 4.15.

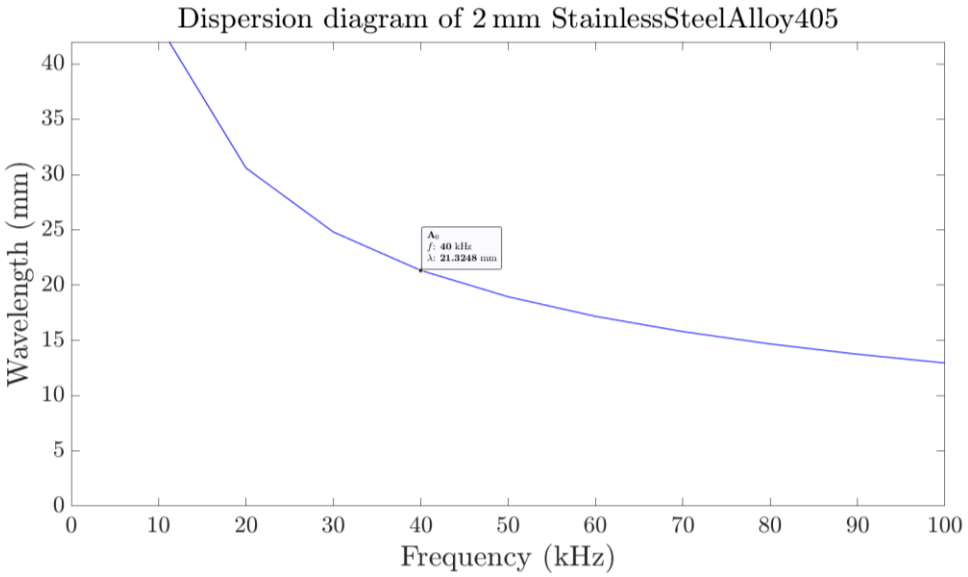


Figure 4.14: Plot of the dispersion curve for the substrate (stainless steel).

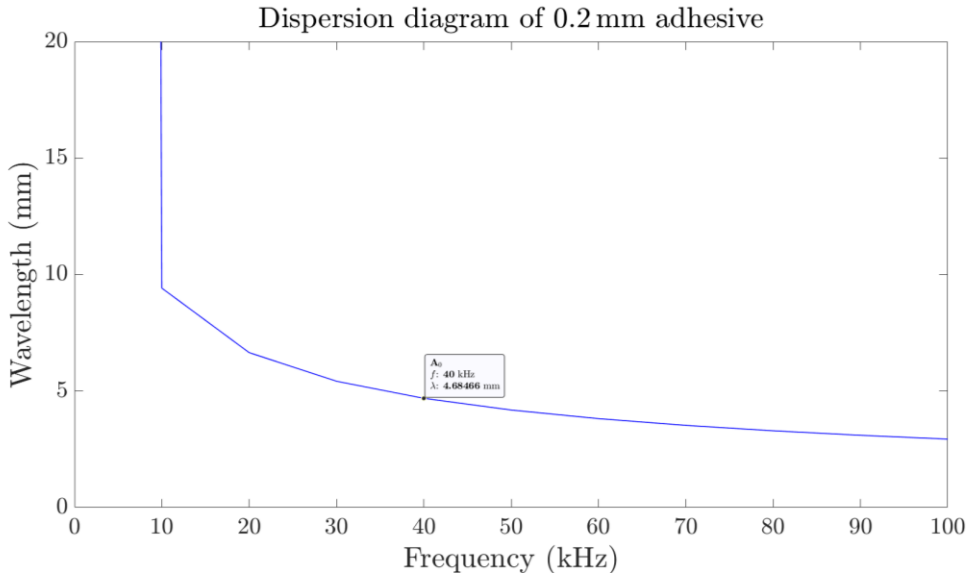


Figure 4.15: Plot of the dispersion curve for the adhesive (AV138).

Once more, from the dispersion curves, it was obtained the corresponding wavelength for the frequency used (40 kHz) and, consequently, the appropriate mesh size, as shown in Table 4.7.

Table 4.7: Corresponding wavelength and advisable mesh size for a 40 kHz frequency in the SLJ model.

| | Stainless Steel | Adhesive |
|---|---|---|
| **Wavelength** | 21.32 mm | 4.68 mm |
| **Mesh size** | 2.132 mm | 0.468 mm |

Due to ABAQUS's limitations, the adhesive's advisable mesh size was not possible to use, since, with a mesh size of 0.4 mm, the number of elements generated was too big for ABAQUS to handle. Given this limitation, the mesh size used was 1 mm, generating a model with 12740 elements.

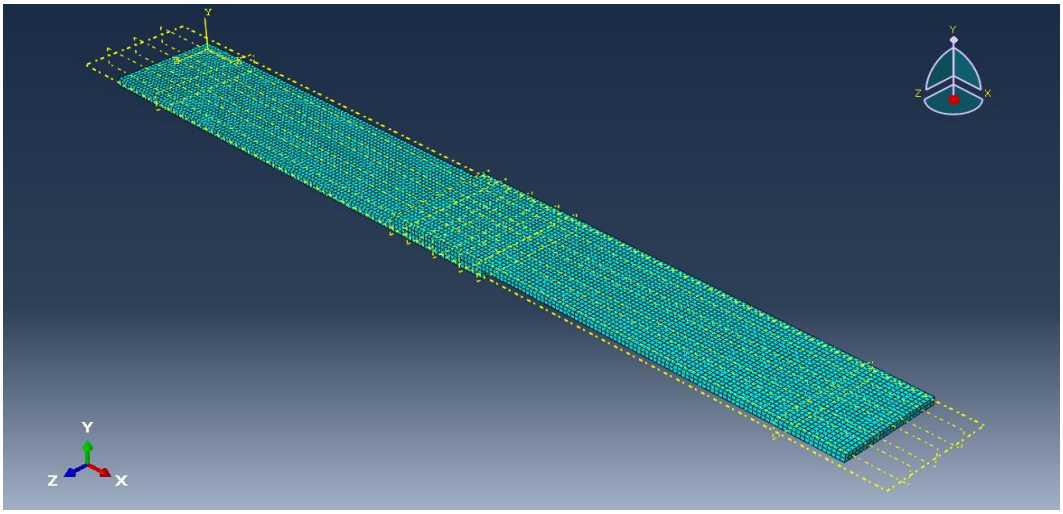


Figure 4.16: Representation of the mesh size chosen for the SLJ model (1 mm).

### 4.2.5 Defect location

In order to analyse the effect of defects in the SLJ, a void was generated within the adhesive layer. This void has a cylindric shape, and that goes throughout the entirety of the adhesive layer's thickness, as shown in Figure 4.17.

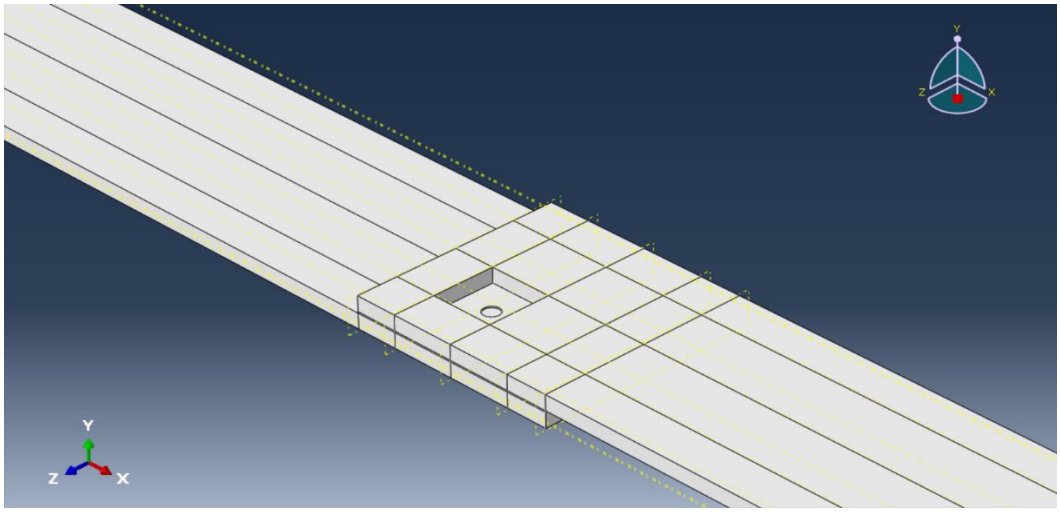


Figure 4.17: Representation of the void with 1mm of diameter embedded in the adhesive layer.

The location of this void was constant in all the simulation being its size the only variable through all the simulations tested. The location of the void is presented in Table 4.8.

Table 4.8: Location of the defect embedded in the adhesive.

| | SLJ_25x25 | | |
|---|---|---|---|
| | **X coordinate (mm)** | **Y coordinate (mm)** | **Z coordinate (mm)** |
| **Defect** | 93.75 | 2 to 2.2 | 8.75 |

### 4.2.6 Results - SLJ

The first simulation was carried out to determine the effect that the adhesive has on LW propagation phenomena. Therefore, two models were compared, one with an adhesive layer of 2 mm thickness with a 25 mm overlap, and another model with the same dimensions as the SLJ model but without the adhesive layer named *SLJ_no_adhesive*, that is, a model with the same dimension of the SLJ but all made of the same material as the substrates (stainless steel). The results are shown in Figure 4.18.

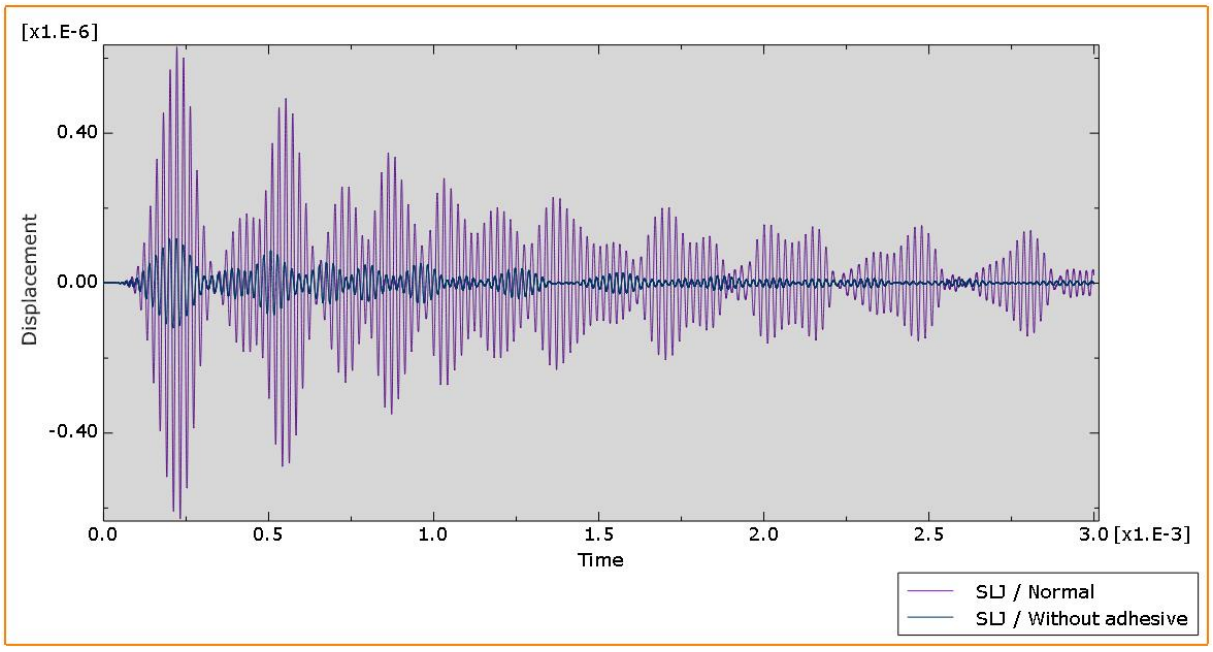


Figure 4.18: Plot of the responses of a normal SLJ and a SLJ without adhesive.

As seen in Figure 4.18, the introduction of the adhesive layer can be seen as a spring when compared to the substrate material. Since,

$$F = K * \Delta x \tag{4.1}$$

where $F$ is the the force implemented in the system by the form of a wave, $K$ the stiffness of the material, and the $\Delta x$ displacement generated by the particles of the material. These results are expectable, since, for the same load magnitude, the adhesive's stiffness is much smaller than that of the substrate, and for the same force applied to both models the displacement ($\Delta x$) would be more prominent in the case of the adhesive.

The next simulation investigated the influence of the void size embedded in the adhesive. In this procedure, three void sizes were simulated (0.2, 0.5 and 1 mm) and compared with the model of a normal SLJ. In Figure 4.19 one can observe the results of this procedure.

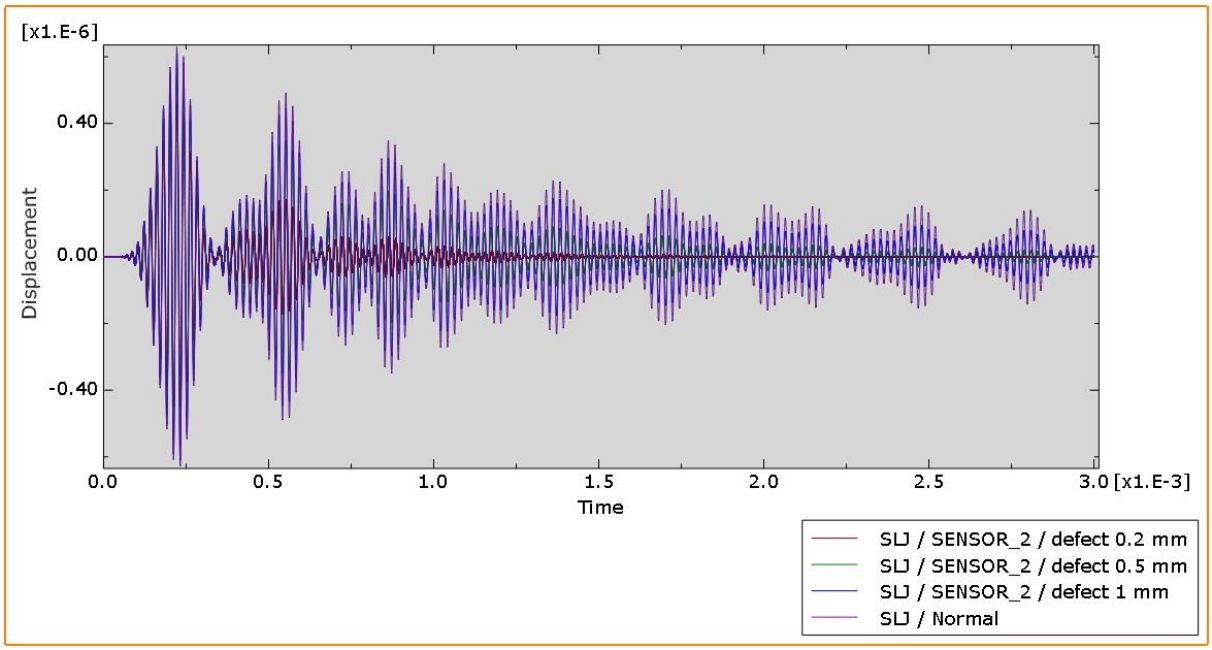


Figure 4.19: Plot showing the influence of the void size in the measured signals.

As Figure 4.19 is not very perceptible, a zoom up was made of the first two modes for a better analysis in Figure 4.20.

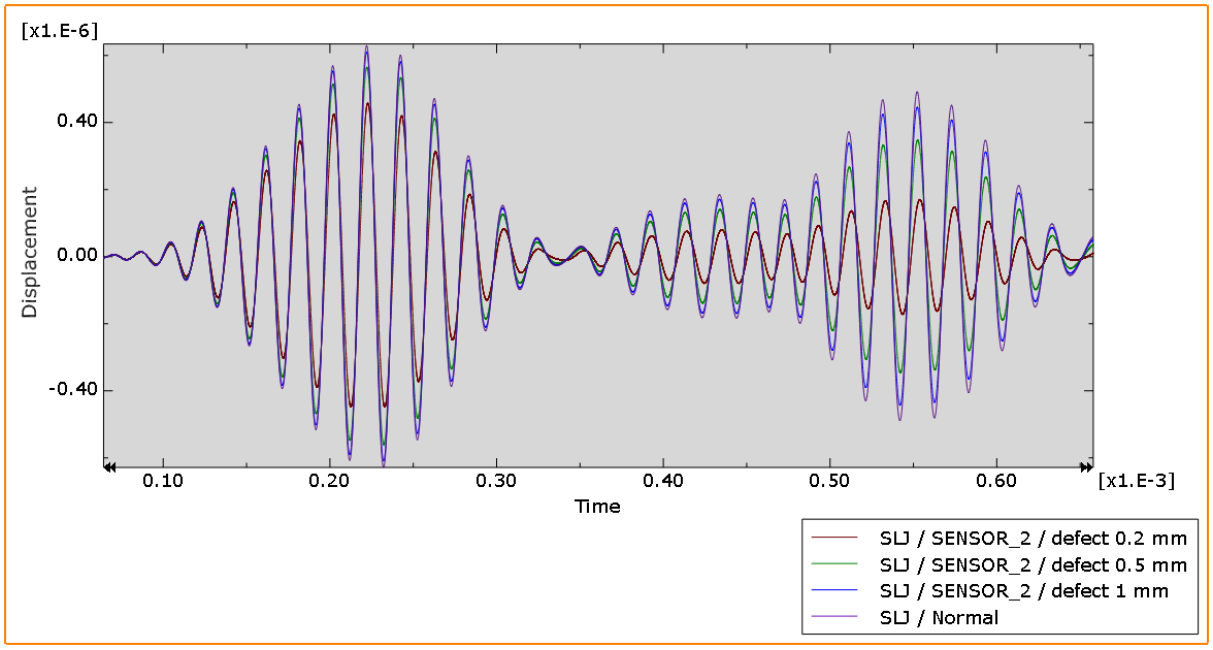


Figure 4.20: Zoomed plot of Figure 4.19.

A clear relation can be identified between the presence and size of the damage and the particle displacement in the piezoelectric sensor. Contrary to what would seem reasonable, the displacement increases and tends to a value similar to the normal SLJ with the increase in void size.

This peculiarity can be explained if one considers that the displacement is affected by many factors. Being the two most predominant ones, the magnitude attenuation of the received signal and the increase in the number of reflection waves due to the presence of damage. The magnitude attenuation would increase with the size of the damage, but on the other hand, a larger void implies a new and more significant boundary condition and, consequently, increases the number of reflected waves.

The graph plotted in Figure 4.20 is a culmination of all the waves that travel thought the receiving sensor, which also means that the higher the number of waves caught by the sensor, the higher the displacement for each given time (since the displacement is given by the sum of all the waves received by the sensor at any given time). Thus, this explains why a bigger defect generates a wave closer to the normal.

The next logical analyses would be to study the damage indices with the data collected for the SLJ model. However, that is not possible since the size of the voids is too small to create a big enough difference between the model with and without the defect. This being said, it does not mean that one cannot obtain a relation with any given damage index. In fact, it is possible that an index based on a frequency domain analysis, or even a culmination of both time and frequency domain, can work. Therefore, more tests need to be done in order to determine this.

## 4.3 Results comparison

Once the data obtained experimental and numerically has been collected, the results were compared, to verify if both procedures produced similar data. In Figure 4.21, the comparison of the SLJ without any defect from both numerical and experimental test is represented.

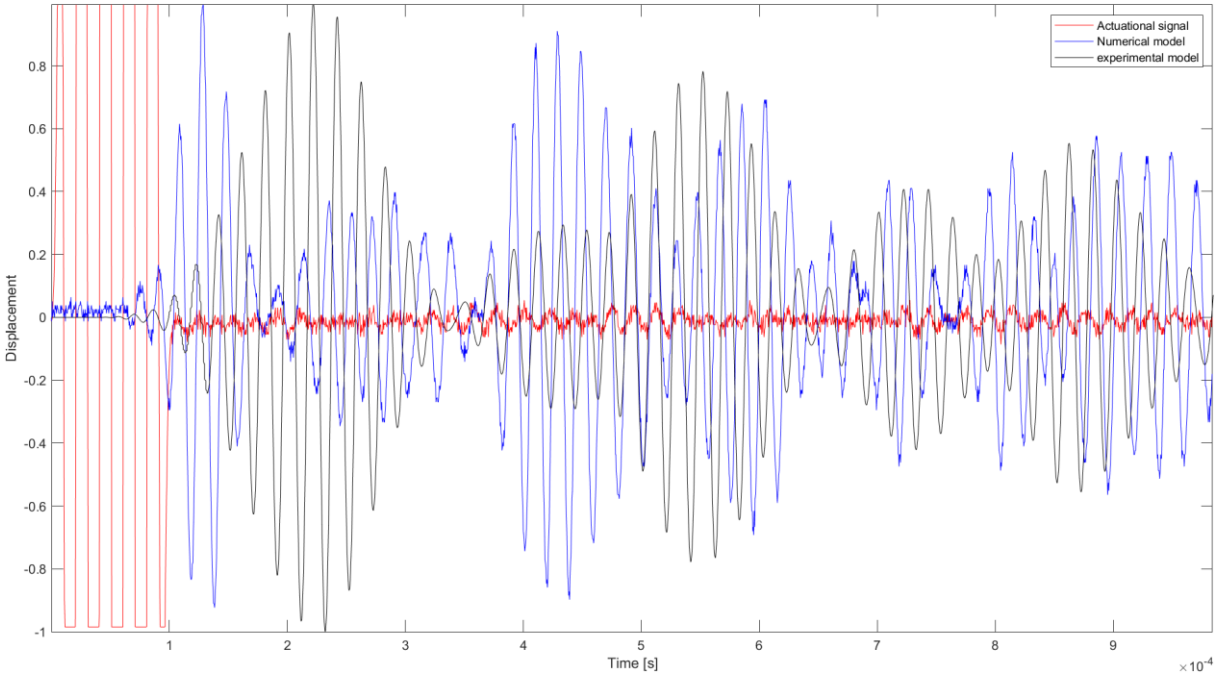


Figure 4.21: Plot comparing the experimental and the numeric results for the standard SLJ.

As seen in Figure 4.21, there is a slight shift in time of the wave modes for both numerical and experimental data. This can be explained by the fact that there is little accuracy in the sensor's attachment for the specimens of the experimental procedure. As such, since PZT sensors can have small deviations in their location, when compared to their nominal placement, the resultant experimental signals may have a different TOF. Therefore, the sensors in both experimental and numerical procedures would not receive the signal in the same instance.

Another aspect that may influence the result comparison is the properties of the adhesive. It is known that elastic properties of the structures vary with the frequency of LW. Consequently, the numerical model used the theoretical values for density, Young's Module and Poisson Ratio for adhesive materials, which may be different than the values observed experimentally.

Figure 4.22 presents the same plot as Figure 4.21. However, the aforementioned time shift was manually adjusted. In this manner, one can see that the signals are extremely similar, therefore proving that the numerical model behaves accordingly to the experimental procedure.

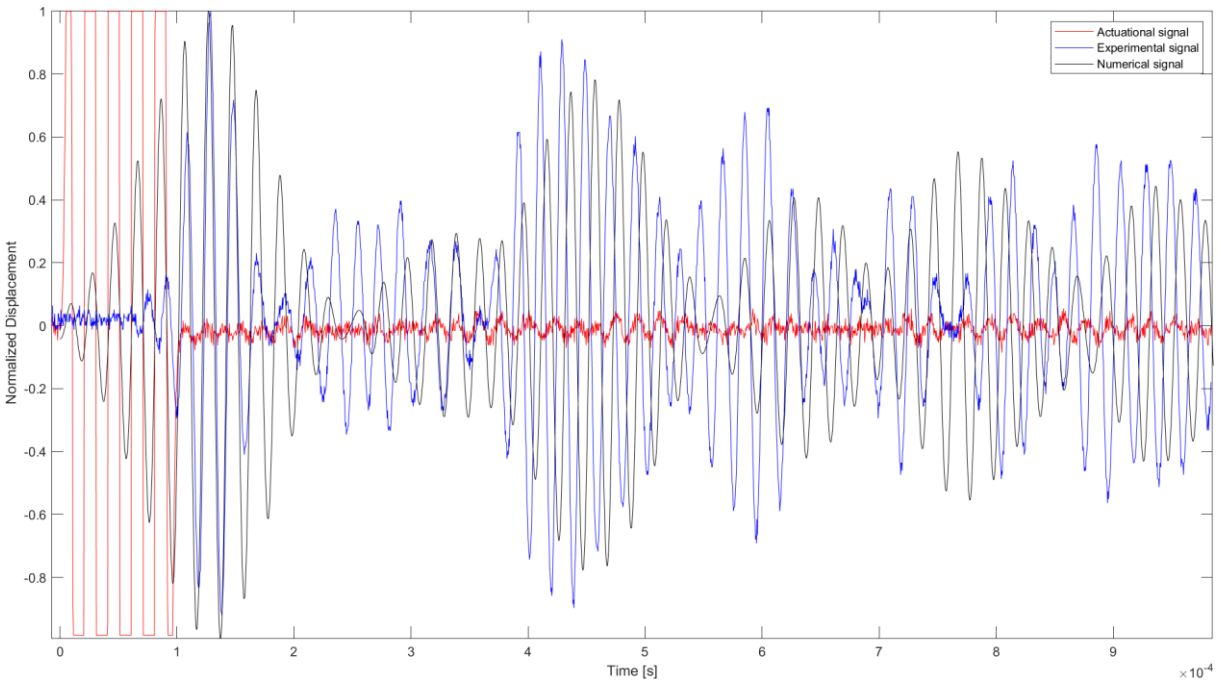


Figure 4.22: Rearranged plot of the numerical and experimental comparison.

# 5 Conclusion and further research

## 5.1 Conclusion

Since the beginning of this dissertation, one of the main goals was to determine if the use of LW's use in NDTs could detect damage in a SLJ. Therefore, many tests were conducted in order to prove this. After a thorough analysis of both the experimental and numerical results, one can take the following conclusions.

Regarding the experimental part, it was possible to detect voids with diameter equal or bigger than 2 mm, since one could observe a clear difference in particle displacement when compared to a non-defect SLJ. Unfortunately, the weak adhesion test was not conclusive, since the difference was not impactful enough to assure its detectability. These conclusions were then proved by conducting destructive tests, where all of specimens have shown a proper recreation of the defect imposed.

Concerning the Numerical simulations, other conclusions can be taken. For straters, it was concluded that this method could locate the defect, which, in this case, was a void, despite their location in the adhesive layer. By taking into consideration the location of the defect relative to the location of the sensors, it was also concluded that the impact on the receiving signal was more significant if the defect was located in the direct path of the wave, generating a more apparent attenuation of particle displacement. Another factor that generated a greater attenuation of the received signal was the size of the void, noting that, with the increase in the void size, a more significant impact can be observed in particle displacement attenuation. On the other hand, the effect of the adhesive in the SLJ were tested, as well as its effect on the LW propagation. This test has shown that the adhesive works as an amplifier of the displacement, due to its elastic properties. This helps in studying the presence of defects, such as voids embedded in the adhesive layer. Therefore, one can conclude that adhesive elasticity has a significant impact on diminishing the data analysis's complexity.

## 5.2 Future research

During this dissertation, several ideas arose, that unfortunately could not be implemented, due to time and resource constraints. This dissertation only analyses the detection of the defects, but this is only the tip of the iceberg regarding these methods' capabilities. LW has the potential to also locate the defect, although to do so, a more significant number of sensors are necessary to define a grid that can triangulate the location of the defect. The determination of the defect's location only makes sense for bigger joints since implementing a grid of sensors requires much space. Therefore, as a future study it is advised to create a bigger joint for implementation of a network of sensors that can determine the damage´s location.

Another future research topic is the detection of other types of defects, like for example, weak adhesion. Although this work tried to detect this defect, the results were not promising. Therefore, a different approach to the method should be considered, such as analysing the sensor data in the frequency domain, possibly with the use of the Fourier Transform.

# References

[1] Kinloch AJ (1987) Adhesion and adhesives: science and technology. Chapman & Hall, London

[2] Adams RD, Comyn J, Wake WC (1997) Structural adhesive joints in engineering, 2nd edn. Chapman & Hall, London

[3] E.Petrie. Handbook of adhesives and sealants. McGraw-Hill Education, 2007, 2007.

[4] Lucas FM Da Silva, Andreas Öchsner, and Robert D Adams. Handbook of adhesion technology. Springer Science & Business Media, 2011.

[5] WA Lees. Adhesive selection. In Adhesives in Engineering Design, pages 92{123. Springer, 1984.

[6] Robert D Adams, Robert D Adams, John Comyn, William Charles Wake, and WC Wake. Structural adhesive joints in engineering. Springer Science & Business Media, 1997.

[7] Robert D Adams. Adhesive bonding: science, technology and applications. Elsevier, 2005.

[8] Sina Ebnesajjad and Arthur H Landrock. Adhesives technology handbook. William Andrew, 2014.

[9] MD Banea and Lucas FM da Silva. Adhesively bonded joints in composite materials: an overview. Proceedings of the Institution of Mechanical Engineers, Part L: Journal of Materials: Design and Applications, 223(1):1{18, 2009.

[10] M. J. Davis and D. A. Bond, 'The importance of failure mode identification in adhesive bonded aircraft structures and repairs', p. 15.

[11] 'Non-Destructive Testing', *Shimadzu*, https://www.shimadzu.com/an/ndi/histry.html (accessed Aug. 05, 2020).

[12] 'History', *NDT- Resourse center*. https://www.nde-ed.org/EducationResources/CommunityCollege/Radiography/Introduction/history.htm (accessed Aug. 13, 2020).

[13] 'NDT Training Institute in Chennai, *Emeral Global Automation India*.

https://egai.in/best-ndt-training-in-chennai/ (accessed Aug. 14, 2020).

[14] J. D. Achenbach, 'Quantitative nondestructive evaluation', *International Journal of Solids and Structures*, vol. 37, no. 1–2, pp. 13–27, Jan. 2000, doi: 10.1016/S0020-7683(99)00074-8.

[15] '10 Common Misunderstandings about Penetrant Testing', *MAGNAFLUX*. https://www.magnaflux.com/Magnaflux/Blog/10-Common-LPI-Misunderstandings (accessed Aug. 14, 2020).

[16] 'Electromagnetic Testing - NDTS', *NDTS India Limited*. https://www.ndts.co.in/electromagnetic-testing/ (accessed Aug. 15, 2020).

[17] '6.4: The Compton Effect - Physics LibreTexts'. https://phys.libretexts.org/Bookshelves/University_Physics/Book%3A_University_Physics_(OpenStax)/Map%3A_University_Physics_III_-_Optics_and_Modern_Physics_(OpenStax)/06%3A_Photons_and_Matter_Waves/6.04%3A_The_Compton_Effect (accessed Aug. 15, 2020).

[18] S. Abbas, F. Li, and J. Qiu, 'A Review on SHM Techniques and Current Challenges for Characteristic Investigation of Damage in Composite Material Components of Aviation Industry', *Matls. Perf. Charact.*, vol. 7, no. 1, p. 20170167, Jun. 2018, doi: 10.1520/MPC20170167.

[19] Lamb, H., 1910, The Dynamical Theory of Sound, Edward Arnold, London, UK.

[20] Worlton, D. C., 1961, "Experimental Confirmation of Lamb Waves at Megacycle Frequencies", Journal of Applied Physics, 32, pp. 967–971.

[21] Hillger, W. and Pfeiffer, U., 2006, "Structural Health Monitoring Using Lamb Waves", 9th European Conference on Non-Destructive Testing - ECNDT, Berlin, Germany.

[22] Nieuwenhuis, J. H., Neumann, J. J., Greve, D. W. and Oppenheim, I. J., 2005, "Generation and Detection of Guided Waves Using PZT Wafer Transducers", IEEE Transactions on Ultrasonics, Ferroelectrics and Frequency Control, 52 (11), pp. 2103-2111.

[23] Edalati, K., Kermani, A., Seiedi, M. and Movafeghi, M., 2005, "Defect Detection in Thin Plates by Ultrasonic Lamb Wave Techniques", 8th International Conference of the Slovenian Society for Non-Destructive Testing - Application of Contemporary Non-Destructive Testing in Engineering, Portoro, Slovenia.

[24] Giurgiutiu, V., 2005, "Tuned Lamb Wave Excitation and Detection with Piezoelectric Wafer Active~Sensors for Structural Health Monitoring", Journal of Intelligent Material Systems and Structures, 16, pp.291.

[25] Gomez-Ullate, Y., Espinosa, F., Reynolds, P. and Mould, J., 2006, "Selective Excitation of Lamb Wave Modes in Thin Aluminum Plates Using Bonded Piezoceramics: FEM Modeling and Measurement", Poster 205, European Conference on Non-Destructive Testing - ECNDT.

[26] Park, G., Sohn, H., Farrar, C. R. and Inman, D. J., 2003, "Overview of Piezoelectric Impedance-Based Health Monitoring and Path Forward", The Shock and Vibration Digest, 35 (6), pp. 451-463.

[27] Giurgiutiu, V. and Bao, J., 2002, “Embedded Ultrasonic Structural Radar with Piezoelectric Wafer Active Sensors for the NDE of Thin-Wall Structures”, ASME International Mechanical Engineering Congress, New Orleans, LA, USA.

[28] B. Rocha, C. Silva, and A. Suleman, ‘Guided Lamb Waves Based Structural Health Monitoring Through a PZT Network System’, p. 8.

[29] J. R. Capinha, ‘Computational and Experimental Studies on Aircraft Structural Health Monitoring Systems’, p. 85.

[30] Peña, J.; Kawieck, G.; Ullate, Y.G.; Freijo, F.M.E.; Melguizo, C.P.; "Low Cost,Low Frequency Phased Array System for Damage Detection in Panels"

[31] D. N. Alleyne, ‘THE NONDESTRUCTIVE TESTING OF PLATES USING ULTRASONIC LAMB WAVES’, p. 251.

[32] X. Zhao *et al.*, “Active health monitoring of an aircraft wing with embedded piezoelectric sensor/actuator network: I. Defect detection, localization and growth monitoring,” *Smart Mater. Struct.*, vol. 16, no. 4, pp. 1208–1217, 2007, doi: 10.1088/0964-1726/16/4/032.

[33] M. Moix-Bonet, P. Wierach, R. Loendersloot, and M. Bach, “Damage Assessment in Composite Structures Based on Acousto-Ultrasonics—Evaluation of Performance,” in *Smart Intelligent Aircraft Structures (SARISTU): Proceedings of the Final Project Conference*, P. C. Wölcken and M. Papadopoulos, Eds., 1st ed., Cham: Springer International Publishing; Imprint; Springer, 2016, pp. 617–629.

[34] B. Eckstein, M. Moix-Bonet, M. Bach, and C.-P. Fritzen, “Lamb wave interaction at debondings due to impact damage in complex stiffened CFRP structures,” in *Health Monitoring of Structural and Biological Systems 2017*, Portland, Oregon, United States, 2017, 101701Q.

[35] Bartle, P. M. (1987). "Acoustic pulsing monitoring: principles operational requirements and potential," The Welding Institute, Abington, Cambridge

[36] Avioli, M. J. **(1988).** "Lamb wave inspection for large cracks in centrifugally cast stainless steel," EPRI report RP2405-23, Georgetown University.

[37] Sache, W., and Pao, Y-H., (1978). "On determination of phase and group velocities of dispersive waves in solids," J. Appl. Phys. vol 49 pp4320-4327.

[38] ‘TGF4000 Series Dual Channel Arbitrary Function Generator | Aim-TTi’, *Aim TTi*. https://www.aimtti.com/product-category/function-generators/aim-tgf4000 (accessed Sep. 25, 2020).

[39]- ‘Overview of Adhesives - Types, Pros and Cons, and Selection Considerations’, 2020. https://www.thomasnet.com/articles/adhesives-sealants/overview-of-adhesives/ (accessed Aug. 25, 2020).

[40] ‘Adhesives Design Toolkit’. http://www.adhesivestoolkit.com/Docs/test/Durability%20Design%20and%20Testing%20-%20Loading%20and%20Failure%20Modes.xtp (accessed Aug. 25, 2020).

[41] ‘Magnetic Field Lines - Definition, Properties, How to Draw - Teachoo’.

https://www.teachoo.com/10694/3113/Magnetic-Field-Lines/category/Concepts/ (accessed Aug. 16, 2020).

[42] 'Principle of magnetic flux leakage. | Download Scientific Diagram'. https://www.researchgate.net/figure/Principle-of-magnetic-flux-leakage_fig12_276831963 (accessed Aug. 16, 2020).

[43] 'Principle of magnetic flux leakage. | Download Scientific Diagram'. https://www.researchgate.net/figure/Principle-of-magnetic-flux-leakage_fig12_276831963 (accessed Aug. 16, 2020).

[44] 'Longitudinal Fields'. https://www.nde-ed.org/EducationResources/CommunityCollege/MagParticle/Physics/LongFields.htm (accessed Aug. 23, 2020).

[45] 'Techshore Inspection Services-Kochi-official blog of Techshore Kerala: What is circular magnetization and how do we do it ?' https://techshoreinspections.blogspot.com/2016/09/what-is-circular-magnetization-and-how.html (accessed Aug. 20, 2020)

[46] 'Techshore Inspection Services-Kochi-official blog of Techshore Kerala: What is circular magnetization and how do we do it ?' https://techshoreinspections.blogspot.com/2016/09/what-is-circular-magnetization-and-how.html (accessed Aug. 20, 2020)

[47] 'Eddy Current Testing: 3D simulation of probe with different excitation frequencies and crack sizes in EMS - Blog'. https://www.emworks.com/blog/ndt/eddy-current-testing-3d-simulation-probe-different-excitation-frequencies-crack-sizes-ems (accessed Aug. 21, 2020).

[48] 'Schematic of a typical ultrasonic testing system. | Download Scientific Diagram'. https://www.researchgate.net/figure/Schematic-of-a-typical-ultrasonic-testing-system_fig15_44848857 (accessed Aug. 23, 2020).

[49] 'Mechanical waves and shear wave induction in soft tissue — Steemit', 2017. https://steemit.com/ultrasonography/@hagbardceline/mechanical-waves-and-shear-wave-induction-in-soft-tissue (accessed Aug. 22, 2020).

[50] Snell's law of reflected and transmitted P-and S-waves at the... | Download Scientific Diagram'. https://www.researchgate.net/figure/Snells-law-of-reflected-and-transmitted-P-and-S-waves-at-the-boundary-between-the-two_fig3_274635028 (accessed Sep. 01, 2020).

[51] -'Applied Sciences | Free Full-Text | Lamb Wave Interaction with Adhesively Bonded Stiffeners and Disbonds Using 3D Vibrometry | HTML'. https://www.mdpi.com/2076-3417/6/1/12/htm (accessed Aug. 27, 2020).